Winter 12-2022

The Influence of Electrical Stimulation Pulse Frequency of Macro-sieve Electrode on Rat Sciatic Nerve Detection Threshold

Jingyuan Zhang

WASHINGTON UNIVERSITY IN ST. LOUIS

McKelvey School of Engineering
Department of Biomedical Engineering

Thesis Examination Committee:

Matthew MacEwan, Chair

Leonard Green

Wilson Ray

The Influence of Electrical Stimulation Pulse Frequency of Macro-sieve Electrode on Rat Sciatic Nerve Detection Threshold

by

Jingyuan Zhang

A thesis presented to
the McKelvey School of Engineering
of Washington University in
partial fulfillment of the
requirements for the degree
of Master of Science

December 2022
St. Louis, Missouri

Table of Contents

List of Figures iv
List of Tables vi
Acknowledgments vii
Abstract viii
Chapter 1: Introduction 1
1.1 Research Objectives 2
1.2 Structure of the Thesis 2
Chapter 2: Background 4
2.1 Limb Loss in U.S. 4
2.2 Upper-Limb Prosthetics 6
2.2.1 Passive 7
2.2.2 Body-powered 7
2.2.3 Electric 8
2.3 Sensory Feedback in Upper-Limb Prosthetics 9
2.3.1 Non-invasive Feedback 11
2.3.2 Invasive Feedback 12
2.4 Structure of Peripheral Nervous System 13
2.5 Electrode Interface for the Peripheral Nervous 14
2.5.1 Extra-neural electrode 15
2.5.2 Inter-fascicular electrodes 16
2.5.3 Intra-fascicular electrodes 17
2.5.4 Regenerative electrodes 18
2.5.5 Macro-Sieve Electrodes 20
Chapter 3: Method 22
3.1 Experimental Apparatus 22
3.1.1 Behavioral Module Hardware 23
3.1.2 Electrophysiological Module Hardware 26
3.1.3 Commutator 27
3.1.4 Programming the Behavioral Module 31
3.2 The Macro-Sieve Electrode Stimuli Module Assembly 32

3.3 Training Rats with Auditory Stimuli 35
3.3.1 Adaptive training 35
3.3.2 Hand-Shaping Stage 36
3.3.3 Auditory Detection Task 37
3.3.4 Bias-correcting Rules 39
3.4 Implantation of the Macro-Sieve Electrode 40
3.5 Methods for Data Collection 47
3.5.1 Resumption of Auditory Training 47
3.5.2 Transferring to Electrical Stimuli 47
3.5.3 The psychometric function 48
Chapter 4: Results and Discussion 51
4.1 Collecting the Data 51
4.2 Analyzing the Data 52
4.2.1 Rat A 52
4.2.2 Rat B 54
4.3 Discussion 57
4.3.1 Detection Thresholds Change 57
4.3.2 Psychometric Function and Data Set 58
4.4 Conclusions 59
Chapter 5: Future Directions 61
5.1 Improvement Scheme 61
5.2 Future Direction 63
References 64

List of Figures

Figure 2.1: Distribution of limb amputations by type in 2005 (adapted from Ziegler-Graham et al.,2008). 5

Figure 2.2: Classification of prosthetics. 7

Figure 2.3: (**A**) A body-powered prosthesis (adapted from Ayub et al., 2017). (**B**) An EMG feedback prosthesis (adapted from Das et al., 2018). 9

Figure 2.4: The feedback loop for prosthesis. 10

Figure 2.5: Classification of prosthetics sensory feedback method**.**..... 11

Figure 2.6: Peripheral nerve interfaces rise with invasiveness (adapted from Navarro et al., 2005). 15

Figure 2.7: (**A**) Cuff Electrode. (**B**) Longitudinal inter-fascicular electrode (LIFE). (**C**) Transverse intra-fascicular multichannel electrode (TIME). (**D**) Utah slanted electrode array (USEA) (adapted from Navarro et al., 2005). (**E**) Regenerative Sieve electrode (adapted from Negredo et al., 2004)..... 19

Figure 2.8: (**A**) The macro-sieve electrode. (**B**) Labeled macro-sieve electrode Platinum-iridium conductors (adapted from Chandra et al., 2021). 21

Figure 3.1 Main pipeline of the experimental. 23

Figure 3.2: (**A**) MED associate SmartCtrl Interface Module. (**B**) Skinner Box. 24

Figure 3.3: (**A**) LZ48M-500 Battery. (**B**) IZ2H-16 Stimulus Isolator. (**C**)RZ5D Base Station. . 27

Figure 3.4: Signal exchange pipeline of the experimental equipment (adapted from Chandra et al., 2021). 32

Figure 3.5: (**A**) Pipeline for the first auditory detection task training stage. (**B**) Pipeline for the second auditory detection task training stage. 39

Figure 3.6: (**A**) A rat in the stereotaxic frame. (**B**) Exposure of the skull. (**C**) Four holes are drilled in the skull and a titanium hex screw is screwed into each hole. (**D**) Place the titanium chamber between the titanium hex screws to ensure proper placement on the skull. (**E**) After the MSE implantation procedure the attached Omnetics connector was passed through the subcutaneous access and placed in the titanium chamber. When filling with acrylic cement, ensure that the locking mechanism is above the upper edge of the titanium chamber. 43

Figure 3.7: Implanted Macro-sieve electrode. 45

Figure 3.8: Pipeline for electrical stimuli detection task. 48

Figure 4.1: (A-E) Psychometric curves of rat A generated by multichannel stimulation at pulse frequencies 50 Hz, 100 Hz, 200 Hz, 400 Hz, and 800 Hz. Error bars represent 95% confidence intervals for the binomial distribution. Threshold, slope, fitting parameters, data dispersion

(Extra variance), threshold difference, and ratio are shown in **Table 4.2**. (**F**) The change of rat A's 75% detection threshold with the change of pulse frequency. Error bars represent 95% confidence intervals. 54

Figure 4.2: (A-E) Psychometric curves of rat B generated by multichannel stimulation at pulse frequencies 50 Hz, 100 Hz, 200 Hz, 400 Hz, and 800 Hz. Error bars represent 95% confidence intervals for the binomial distribution. Threshold, slope, fitting parameters, data dispersion (Extra variance), threshold difference, and ratio are shown in **Table 4.3**. (**F**) The change of rat B's 75% detection threshold with the change of pulse frequency. Error bars represent 95% confidence intervals. 56

List of Tables

Table 2.1: Estimates of Prevalence by Type and Level of Limb Loss and Etiology (in thousands): Year 2005, United States (Ziegler-Graham et al., 2008). 5

Table 3.1: Materials used in behavioral module hardware (adapted from Chandra et al., 2021). 25

Table 3.2: Materials used in electrophysiologica module hardware (adapted from Chandra et al., 2021). 27

Table 3.3: Channel mappings for commutator Omnetics connector (adapted from Chandra et al., 2021). 30

Table 3.4: Materials used in commutator (adapted from Chandra et al., 2021). 30

Table 3.5: Channel mappings for macro-sieve electrode and DB25 connector (adapted from Chandra et al., 2021). 34

Table 3.6: Materials used in macro-sieve electrode stimuli module (adapted from Chandra et al., 2021). 34

Table 3.7: Materials used in the implantation of the macro-sieve electrode procedure (adapted from Chandra et al., 2021). 41

Table 4.1: Schedule of training, surgery, and data collection for rats A and B. 51

Table 4.2: Threshold, slope, fitting parameters (α β, γ, λ), data dispersion (Extra variance, η), threshold difference, and ratio of rat A generated by multichannel stimulation at pulse frequencies 50 Hz, 100 Hz, 200 Hz, 400 Hz, and 800 Hz shown in **Figure 4.1**. 54

Table 4.3: Threshold, slope, fitting parameters (α β, γ, λ), data dispersion (Extra variance, η), threshold difference, and ratio of rat A generated by multichannel stimulation at pulse frequencies 50 Hz, 100 Hz, 200 Hz, 400 Hz, and 800 Hz shown in **Figure 4.2**. 56

Acknowledgments

Thanks to all those involved in this project, without whom the work presented in this paper would not have been possible. Many thanks to my PI, Dr. Wilson Ray, and Dr. Matthew MacEwan, for their guidance, encouragement, and financial support throughout the project. I would also like to sincerely thank the graduate Nikhil Shiva Chandra, who built and programmed the instrumentation system used in this project. I would also like to thank Dr. Leonard Green for his extensive assistance in the design of behavioral experiments and Dr. Ying Yan, the chief scientist of the laboratory, for his assistance in animal surgery. Finally, thanks to our lab members Nathan Birenbaum, Yameng Xu, Michael Rosario, Eddie Hong, and Lili Hostetler for their help. It was a pleasure working with all of you!

Jingyuan Zhang

Washington University in St. Louis

December 2022

ABSTRACT OF THE THESIS

The Influence of Electrical Stimulation PF of Chronic Macro-sieve Electrode on Rat Sciatic Nerve Detection Threshold

by

Jingyuan Zhang

Master of Science in Biomedical Engineering

Washington University in St. Louis, 2022

Associate Professor Matthew MacEwan, Chair

To achieve dexterous manipulation of objects through prosthetics, encoding stimulus parameters into sensory feedback that upper-limb prosthetics users can interpret is critical. From a neurophysiological perspective, the evoked sensation depends on many factors, such as stimulation current, voltage, frequency, and waveform, which significantly affects the evoked sensation. The central goal of this project is to test the effects of various macro-sieve electrode (MSE) stimulation pulse frequency (PF) configurations on the user's detection thresholds. MSE-implanted rats performed a yes/no discrimination task based on a "multi-channel" stimulation configuration that simultaneously delivered equal currents to all eight MSE channels. The resulting data from the detection task generated psychometric curves that described the relation between stimulation amplitude and forced-choice response in the rats. The results showed that the frequency of multi-channel electrical stimulation signals considerably affected the detection thresholds. In addition, the effect of electrical stimulation PF on detection thresholds was not linear but quadratic, representing a possible plateau for this form of stimulation. The specific cause of this finding and the development of an accurate quantitative law, however, remain to be

determined. These results represent an essential theoretical basis for establishing the feasibility of MSE as a complex sensory feedback interface.

Chapter 1: Introduction

To achieve dexterous manipulation of objects through prosthetics, sensory feedback is crucial for upper-limb prosthetics. However, encoding stimulus parameters into sensory feedback that users can interpret intuitively remains a significant challenge. From a neurophysiological perspective, the evoked sensation depends on many factors. In the case of using the same type of electrodes, the parameters of the electric stimulus, such as current, voltage, frequency, and waveform, will significantly affect the evoked sensation (Geng et al., 2018). Li et al. published a study in 2018 in which they attempted to noninvasively induce sensory feedback in the phantom finger area (PFT) near the amputee's stump via electrical nerve stimulation (TENS). Pulse amplitude (PA), pulse frequency (PF), and pulse width (PW) were modulated to assess the detection threshold, perceived touch intensity, and just noticeable difference (JND) of phantom sensation (Li et al., 2018). In the same year, Geng et al. (2018) published a study using subcutaneous electrical stimulation to assess sensory feedback in prosthetic limbs. Detection Threshold (DT), Pain Threshold (PT), Perceivable Difference (JND), and Evoked Sensory Quality, Comfort, Intensity, and Position were assessed in 16 healthy volunteers using subcutaneous stimulation of the ventral and dorsal forearms (Geng et al., 2018). The results of both papers show that electrical stimulation's pulse frequency (PF) l stimulation can affect users' sensory feedback perception gate value. However, the reasons and rules for this effect still need to be clarified. Considering the direction of electrode performance, if the electrode is less invasive, it will show such a rule. Then the highly invasive electrodes with high spatial discrimination should show more obvious similar rules when using the same stimulation configuration.

Our current research on Macro-sieve Electrodes (MSE) is focused on whether it can induce high-fidelity sensation while maintaining a low current level that does not damage nerve tissue and

has successfully achieved some results. However, limited by the current recording and analysis method, our current results have only shown us the thresholds of multi-channel and single-channel stimulus at 50 Hz. The rest of the thresholds' changes at other frequencies remains unclear. Therefore, a more efficient data recording and analysis method is needed to analyze the effect of different PF on the stimulus threshold.

1.1 Research Objectives

The project is an extension of the Macro-Sieve Electrode Stimulation Project, the central goal is to test the effects of different various MSE stimulation pulse frequency (PF) configurations on detection thresholds and slopes based on existing data and testing methods. MSE-implanted rats will perform a yes/no discrimination task based on a "multi-channel" stimulation configuration that simultaneously delivers equal currents to all eight MSE channels. The resulting data can be processed to generate psychometric curves that describe the relationship between stimulation amplitude function and forced choice response in rats. By calculating these curves, the detection threshold of the electrical stimulus configuration of the rat can be displayed, that is, the lowest stimulus level that the rat can feel under the electrical stimulus condition. After the curve calculation and fitting are completed, the project will analyze the obtained result to explore the relationship between the PF and the detection threshold of electrical stimulation.

1.2 Structure of the Thesis

This paper is divided into five chapters, describing the effect of the PF of MSE electrical stimulation on the rat's detection threshold. Chapter 1 (i.e., This chapter) introduces the research topic and outlines the research objectives.

Chapter 2 describes the types of upper-limb prosthetics and the importance of sensory feedback to upper-limb prosthetics. Then, the chapter describes the organization of peripheral nerves. Finally, it outlines the development of the different types of electrodes used to provide sensory feedback today.

Chapter 3 describes the methods for training rats to perform a detection task using auditory stimuli, the surgical procedure, postoperative retraining, and how to transition from auditory to electrical stimulation. Finally, it explains the derivation of the formula used to generate the psychometric curve and the fitting method.

Chapter 4 describes the execution of this experiment with two rats over one year. Next, it details the data collection and analysis results for each rat. Finally, it evaluates the reliability and limitations of the analytical results.

Chapter 5 describes the improvement method of this experiment and the direction of future research. First, it provides suggestions for improving the credibility of the data. Then, it summarizes the general planning of future research directions, which will be the main development direction of subsequent experiments.

Chapter 2: Background

The following guidelines offer you some degree of flexibility in formatting your thesis or dissertation. Whichever options you choose to use, you must use them consistently throughout the document.

2.1 Limb Loss in U.S.

Limb loss is one of the most severe problems worldwide, mainly caused by trauma, medical disease, or congenital diseases (Das et al., 2018). According to statistics, the annual direct health care costs related to limb loss total nearly 8 billion U.S. dollars. In addition, patients with limb loss often struggle with multiple chronic health conditions and have a higher mortality rate than many common chronic diseases. According to research, the incidence of cardiovascular disease, obesity, joint and bone problems, depression, and emotional distress in limb loss patients is higher than in ordinary (Sheehan & Gondo, 2014).

Based on statistics, as of 2005, an estimated 1.6 million people lost limbs. Amputations secondary to vascular disorders accounted for the majority (54%) of cases, limb loss secondary to trauma accounted for another 45% of prevalent cases, and cancer accounted for the remaining less than 2%. Of these 1.6 million, 65% lost lower limbs, of which 39% were major amputations. In contrast, only 3% of patients who lost an upper limb were classified as major. The prevalence of limb loss is estimated to increase from 1.6 million in 2005 to 3.6 million by 2050 (Ziegler-

Graham et al., 2008).

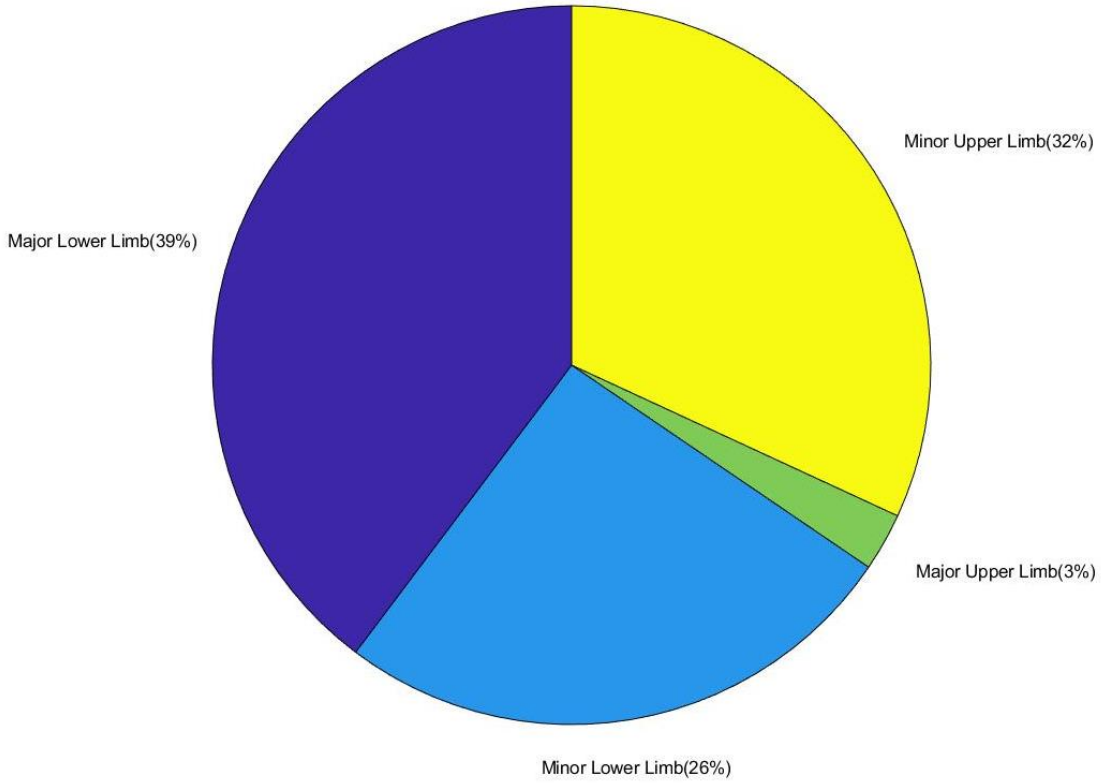

Figure 2.1: Distribution of limb amputations by type in 2005 (adapted from Ziegler-Graham et al.,2008).

Table 2.1: Estimates of Prevalence by Type and Level of Limb Loss and Etiology (in thousands): Year 2005, United States (Ziegler-Graham et al., 2008).

		Lower Limb		**Upper Limb**	
Ethology	Total	Major	Minor	Major	Minor
Dysvascular disease	846	504	302	5	34
Trauma	704	106	101	34	464
Cancer	18	13	1	2	1

All etiologies	1568	623	404	41	500

2.2 Upper-Limb Prosthetics

Prosthetics can be divided into various categories according to structure, function, amputation site, power source, and material. The most common classification method is to divide the prosthesis into the upper-limb prosthesis and lower-limb prosthesis according to the amputation site. This article will focus on the common types of modern upper-limb prostheses. Prosthetics are very old, the first written record of an upper limb prosthesis is documented in a book published in France in 1579, written by the French surgeon Ambroise Paré, part of it describes some of the prosthetics he fitted to patients (Hernigou, 2013). Functionality and toughness were the main criteria for early prosthetic designs, with some designs having articulations that could be locked by a spring-ratchet mechanism via a metal lever and operated by a supporting hand (Das et al., 2018). However, due to era and technical limitations, these upper-limb prosthetics could not provide proper grip and lacked design sensitivity. With the development of biomechanics and engineering and the improvement of productivity, modern upper-limb prosthetics have been able to meet the complex functional needs of professional and amateur users. Modern upper limb prostheses can be divided into passive and active according to the driving method. Active upper-limb prostheses can be divided into body-powered and electric according to their power source (Trent et al., 2019; Schultz & Kuiken, 2011).

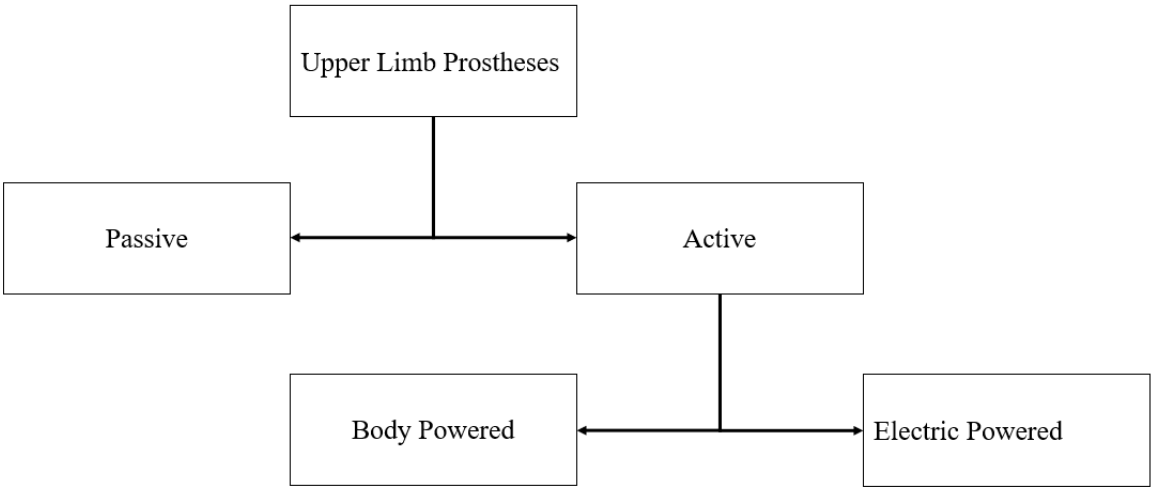

Figure 2.2: Classification of prosthetics.

2.2.1 Passive

Passive prosthetics are static or positioned, primarily used to restore the anthropomorphic limb length needed by the user to carry or stabilize objects. Current passive prosthetics are mostly made of flexible latex, rigid PVC, or silicone materials and can complete the feedback of electronic products. Because passive prostheses do not actively move, passive prostheses have relatively limited grasping capabilities compared to active prostheses. The most significant advantage of passive prosthetics is that they can be designed to look natural. The natural appearance helps the user restore their body image and reduce unwanted attention. However, the formation of a passive prosthesis is an adjunct to its function, which is still used to protect sensitive areas on the residual limb and restore limb length (Trent et al., 2019).

2.2.2 Body-powered

Body-powered prostheses are currently the popular choice for upper-limb prostheses, and as of 2003, they remain the first choice in most pediatric clinics in the United States. Body-powered prosthetics use wire harnesses to capture proximal body motion, and the other ends of the wires

are attached to hooks or bionic hands and affect their movement. Body-powered prosthetics have several advantages over types, such as lighter weight, greater durability, greater tolerance to environmental conditions, and lower initial price and maintenance costs. However, despite the many advantages of body-powered prosthetics, there are also significant disadvantages. Common problems reported with body-powered prostheses include excessive wearing temperature, clothing fraying, faulty wires, unsightly appearance, slow movement, difficulty cleaning, insufficient grip strength, and discomfiture or breakage of the harness (Biddiss & Chau, 2007; Trent et al., 2019).

2.2.3 Electric

Electric prostheses use motors to achieve movement and are typically powered by a rechargeable battery system. Depending on the design, motorized prosthetics can be controlled in of several different ways, including electromyography (EMG) signals, servos, linear potentiometers or sensors, force-sensitive resistors, rocker switches, push button switches, and wire pull switches. Among them, EMG signal control is the most common, and the general idea of EMG signal control is to use electrodes to measure muscle action potential. EMG prosthesis use surface electrodes to pick up signals at different locations on the skin surface and amplify them for motor control. Electric prostheses usually have greater pinch strength, ease of manipulation, and no need for straps than other types of prostheses. However, electric prosthetics also have higher weight and maintenance costs. However, electric prosthetics also have higher weight and maintenance costs. Currently, the biggest problem with electric prosthetics is its control accuracy and sensory feedback for complex movements, so research in related directions has become popular in recent years (Biddiss & Chau, 2007; Das et al., 2018; Trent et al., 2019).

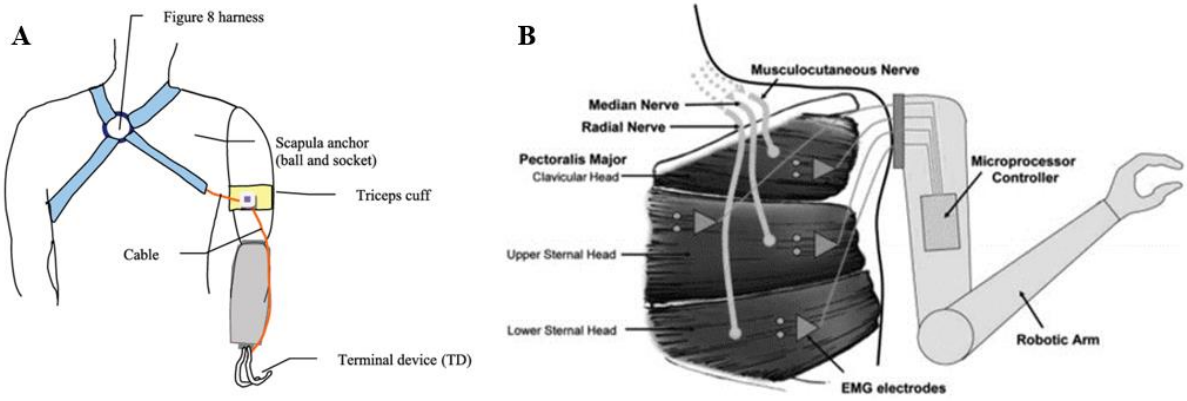

Figure 2.3: (**A**) A body-powered prosthesis (adapted from Ayub et al., 2017). (**B**) An EMG feedback prosthesis (adapted from Das et al., 2018).

2.3 Sensory Feedback in Upper-Limb Prosthetics

The functionality of the upper-limb prosthesis depends on the ergonomics between the user and the prosthesis. However, imitating the performance of human hands and arms is still the primary technical problem. Anatomically, a typical hand is capable of coordinated movement in 27 degrees of freedom to perform force-based grasping functions and highly coordinated precision movements (Schofield et al., 2014). Control of grasping and manipulating arms and palms relies heavily on human tactile feedback. Therefore, if an upper-limb prosthesis is to mimic a human hand and arm as closely as possible, the prosthesis should be able to detect physical interactions with the environment and communicate this information to the user (Antfolk et al., 2013).

Currently, in clinical practice and academic research, there are two classification methods for the feedback mode of prosthetics. The first method is based on the user's experience feedback signal method, and the feedback method is divided into modality matching, and body matching methods (Schofield et al., 2014). The second method is to divide the feedback method into invasive and non-invasive according to the installation position of the feedback device (Svensson

et al., 2017). This article will take the second classification method as the main body and combine it with the first method to briefly describe the current popular feedback methods.

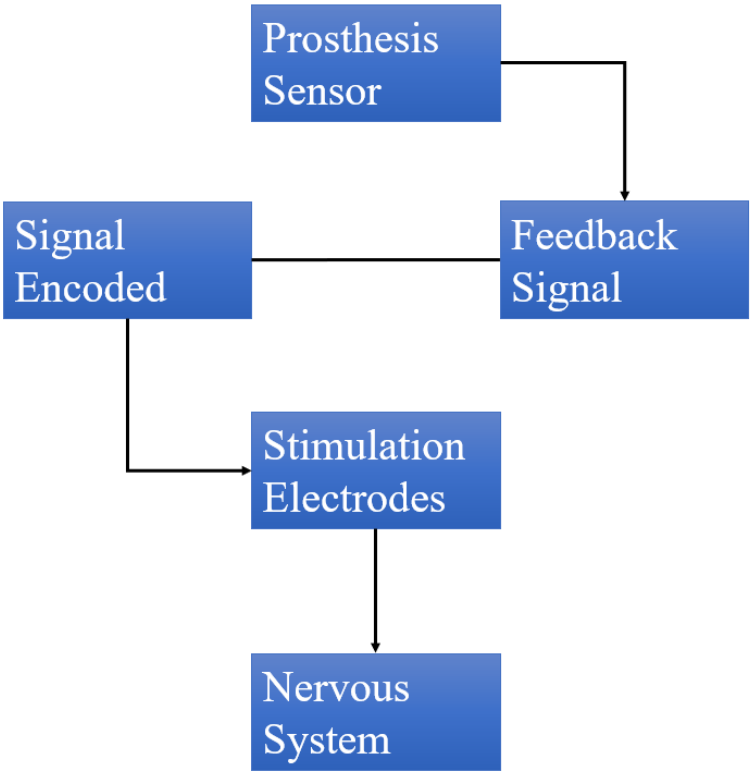

Figure 2.4: The feedback loop for prosthesis.

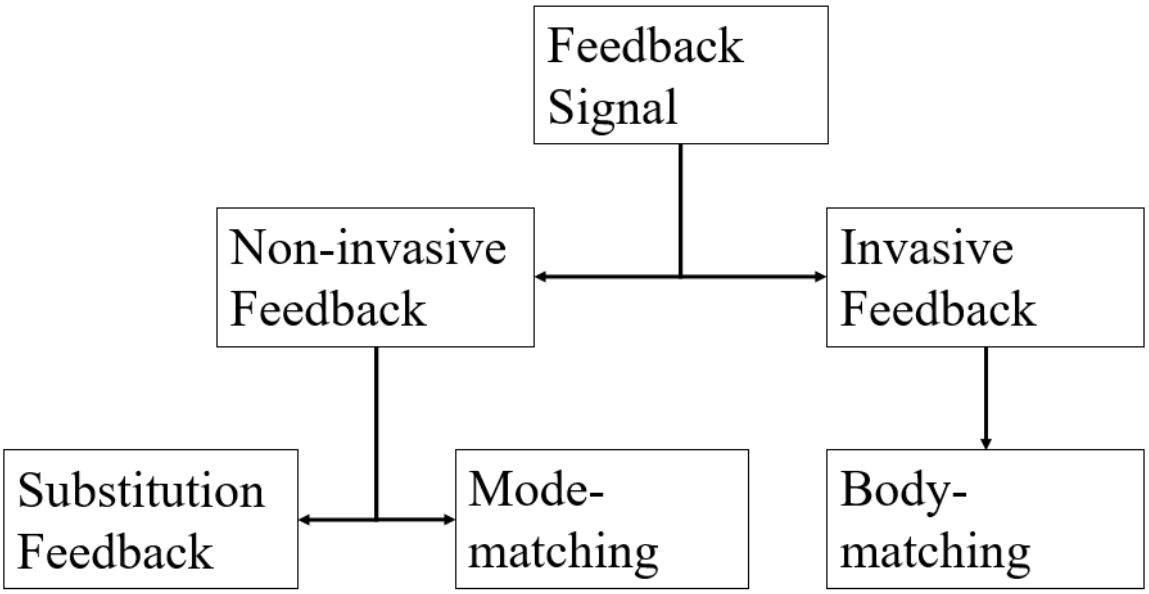

Figure 2.5: Classification of prosthetics sensory feedback method**.**

2.3.1 Non-invasive Feedback

At present, in clinical practice, the feedback of prosthetics is still mainly non-invasive, and the feedback form of its signal is mainly substitution or modality matching. Substitution feedback conveys the prosthesis's status to the user through tactile or auditory feedback from other parts. The most common approach is to use vibration, electric or auditory stimulation to convey tactile information from the prosthetic to the user (Schofield et al., 2014). In theory, substitutions are the most direct way to give feedback since they do not consider modality or body matching. However, the success of this approach depends on the user's ability to subjectively interpret the type and location of stimuli and associate them with the prosthetic. Therefore, users may be confused or feel uncomfortable due to the similar intensity of feedback (Svensson et al., 2017).

Mode-matching feedback is another standard non-intrusive feedback method. This feedback method matches the information conveyed to the user regarding somatosensory feelings. For example, with the body power device, the user can perceive the state of the prosthesis and the grip strength by controlling the reaction force transmitted by the cables and straps on the body (Antfolk et al., 2013). Since the information conveyed by the modal matching feedback signal to the user is matched in a sense, the user does not need to interpret the feedback signal too much. Therefore, mode-matching feedback tends to have lower cognitive requirements than substitution feedback. Thus, in some cases, such as body-powered prosthetics, modality-matching feedback may be more reliable than substitution feedback (Schofield et al., 2014).

2.3.2 Invasive Feedback

Invasive prosthetic feedback is still mainly in the academic research phase, with only a few earlier proposed approaches entering clinical trials. The signal feedback form of intrusive prosthetic feedback is classified as body-matching feedback. The body-matching feedback method implants electrodes into the user's body and enables the amputee to feel the information feedback from the prosthesis through electrical stimulation (Schofield et al., 2014). The effect of invasive prosthetic feedback is mainly affected by the electrode implantation site and the electrode type. Currently, the two most mainstream implantation sites are peripheral nerves and the somatosensory area of the brain. According to research in recent years, neural coding is easier to understand in peripheral nerves than in the brain, and the risks caused by surgery are also more minor (Svensson et al., 2017). Furthermore, body-matching feedback can relieve a substantial cognitive load on the user, as stimulation from the prosthetic sensor will be perceived as a physiologically matched position for the missing limb. In other words, the user only needs

less training and attention to interpret the feedback signal from the prosthesis (Schofield et al., 2014).

2.4 Structure of Peripheral Nervous System

The somatic peripheral nervous system (PNS) consists of sensory afferent fibers that connect receptors to the central nervous system (CNS) and motor efferent fibers that connect the CNS to muscles or glands (Hadzic, 2007). From proximal to distal, which mainly contains ventral and dorsal roots, roots, spinal nerves, dorsal and ventral branches, nerve plexuses, individual peripheral nerves, and their branches. This system contains a variety of combinations of nerve fibers, including myelinated and unmyelinated, somatic, and autonomic (Stewart, 2003). On the outside of each peripheral nerve is a dense sheath of connective tissue called the epineurium. The epineurium wraps individual nerve fibers (myelinated and unmyelinated) grouped into fascicles, known as fascicles. Each fascicle is surrounded by a perineurium consisting of neurolemma cells and a collagen layer. Individual nerve fibers within the fascicles are embedded in loose connective tissue (endoneurium) to fill the space around the neurolemma (Hadzic, 2007; Stewart, 2003).

There have been debates in academic circles about the arrangement of nerve bundles, mainly consisting of two opposing views. The early view thought that nerve bundles were arranged like cables. That is, the fibers of a single peripheral nerve branch are consistently arranged in a discrete state throughout the whole nerve length. The latter view holds that a single nerve fiber has many branches and branches that split and recombine as the peripheral nerve expands. This mixing gives the nerve a plexiform appearance (Stewart, 2003).

2.5 Electrode Interface for the Peripheral Nervous

Feedback electrode availability for prosthetics depends on two main properties. The first is the biocompatibility of the electrode. From the perspective of materials science, electrodes will be in a specific chemical environment for a long time after they are implanted in the human body. During this period, the materials that make up the electrodes will gradually corrode over time. Therefore, a significant characteristic is whether the electrode can be used in the body for a long time and cause as minor chronic physiological or tissue damage to the surrounding tissue as possible. This property is related to whether the electrode should continue to provide feedback signals for the prosthesis for as long as possible (Rijnbeek et al., 2018). Second is the number of interfaces between the electrodes and the nerve fibers. A more significant number of interfaces means more options for prosthetics with different sensations and controls that can provide feedback on different areas of the limb. From the perspective of implantation technology, the more invasive nerve electrodes have more interfaces, but the relative damage to the nerves is also more significant (Rijnbeek et al., 2018; Russell et al., 2019).

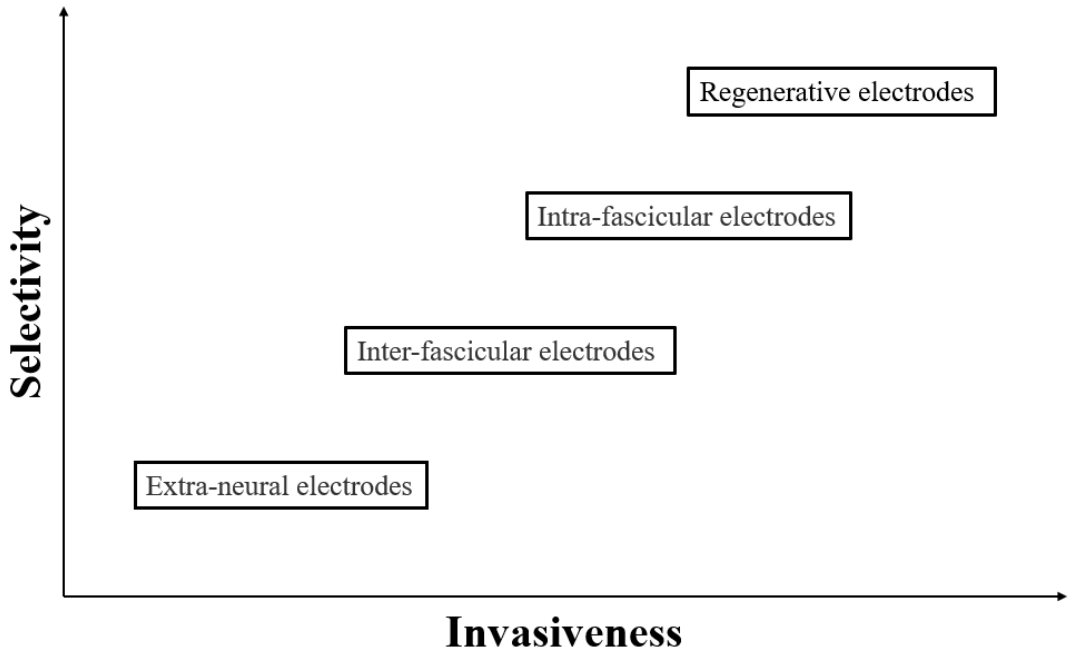

Figure 2.6: Peripheral nerve interfaces rise with invasiveness (adapted from Navarro et al., 2005).

2.5.1 Extra-neural electrode

Extra-neural electrodes are the least invasive electrodes placed on the outer surface of the nerve just outside the epineurium. There are four main types of Extra-neural electrodes: the epineural electrode, the helical electrode, the book electrode, and the cuff electrode. In this section, only the most representative and widely studied electrode the cuff electrode (Russell et al., 2019; Yildiz et al., 2020).

After implantation, the cuff electrode is wrapped around the surface of the nerve, and it measures the difference in the external potential of the nerve during the propagation of the action potential. The cuff electrode, the most widely studied peripheral nerve interface, has many different variants, and these designs are named according to their morphological properties. One typical

design is called a split cylinder cuff electrode. This electrode is usually a cylindrical tube cut longitudinally and placed around the nerve with or without sutures. The electrical contacts of the cylindrical tube are concentric or longitudinal, and their size must be predetermined according to the target nerve. Another more common variant is the flat interface nerve electrode (FINE), which differs from the cuff electrode in its rectangular shape. Because of its rectangular structure, it can use less force and reshape nerves into a flattened oval shape to move axons closer to electrical contacts, facilitating selective recording and stimulation (Rijnbeek et al., 2018; Yildiz et al., 2020).

Because the cuff electrodes are relatively non-invasive, they last longer than other designs. Studies have shown that a large number of long-term cuff electrodes implanted in the human body's peripheral nerves can work stably for up to 10.4 years. However, because cuffs do not penetrate the epineurium, it is difficult to achieve highly selective recording and complex signal feedback from a single fascicle (Rijnbeek et al., 2018).

2.5.2 Inter-fascicular electrodes

In neuroanatomy, groups of motor neurons are interspersed in fascicles that vary in their location in the nerve. Longitudinal inter-fascicular electrodes (LIFE) were developed to protect the integrity of the fascicles by not penetrating the fascicles based on proximity to these fascicles. Electrodes are surgically inserted with wires penetrating the epineurium until it reaches the fascicles. It is inserted along the fascicles without penetrating the perineurium. As a result, electrodes occupy the space between fascicles to record/stimulate central axons (Russell et al., 2019; Rijnbeek et al., 2018; Yildiz et al., 2020).

Early LIFE was very stiff due to material constraints. This results in relative movement of the electrodes within the fascicle, which leads to gradual drift and signal degradation of the recorded

nerve fiber population. Also, although the LIFE electrodes consist of 8 individual contact points, the electrodes are only close to some fascicles due to the longitudinal distribution of LIFE. Therefore, it is still difficult to selectively stimulate or record individual tracts. Due to (Rijnbeek et al., 2018).

2.5.3 Intra-fascicular electrodes

Like inter-fascicular electrodes, intra-fascicular electrodes penetrate the epineurium directly into or through the fascicles. While this method is known for its spatial resolution and selectivity, it is more invasive and has the potential to damage nerves. According to their connection method, there are two main types of intra-fascicular electrodes (LIFE) and transverse intra-fascicular multichannel electrodes (TIME). Simultaneously penetrating microelectrode arrays (MEAs) can be considered a third type because they contain arrays of many tiny electrodes arranged in an orderly manner. As a particular category, LIFE can be used as inter-fascicular or intra-fascicular electrodes depending on its material, implantation method, and length (Russell et al., 2019; Yildiz et al., 2020).

When implanted, TIME is inserted laterally into the nerve and exits the nerve again. The TIME electrode consists of a thin strip polyimide substrate with platinum electrode sites. Fold the base to align multiple electrodes and pass the folded base laterally across the nerve between the fascicles. TIME thus has electrical contact interfaces with different subsets of axons. Since a thin device may be sufficient to connect several groups of nerve fibers, surgical implantation trauma is minimized, avoiding potential nerve damage. In addition, due to TIME's lateral location in the nerve, its contact points are located near multiple fibers on the nerve belonging to different tracts, which allows TIME to record and stimulate individual tracts more specifically than LIFE (Rijnbeek et al., 2018; Yildiz et al., 2020).

Another method of intra-beam connection is the use of laterally inserted penetrating microelectrode arrays (MEAs). The MEA consists of a plane with many tiny electrodes constructed of various metals capable of recording and stimulating the central and vast spaces of the PNS. Utah Slanted Electrode Array (USEA) is currently the most effective among the many designs. The USEA contains 100 individual microelectrodes spaced 400 µm apart on a 10 x 10 grid. In experiments, a single USA covered almost the entire depth and width of the feline sciatic nerve, maintaining contact with many fibers. However, in terms of longevity, the array has two significant problems. First, USEA will need many wires to connect due to the number of electrodes. Such characteristic makes the USEA more fragile than other electrodes. Second, a large number of penetrating electrodes can cause chronic damage to the nerve and connective tissue formation due to the movement of surrounding tissue. Therefore, the recording performance of USEA decreases over time as connective tissue gradually forms (Rijnbeek et al., 2018; Yildiz et al., 2020).

2.5.4 Regenerative electrodes

The final electrical interface method for the PNS is the regenerative electrode, which uses regeneration to grow the nerve around the electrode instead of puncturing it. This type of electrode can make contact with a large number of axons. Regenerative electrodes can be divided into two types of structures, sieve electrodes and regenerative multi-electrode arrays (Yildiz et al., 2020). Sieve electrodes consist of a microporous structure covered with a conductive material and placed between the ends of a severed nerve when implanted. The severed nerve regenerates through the microporous structure, which can then be used to elicit or record from the nerve. The regenerative multi-electrode array is designed by having multiple USEA-like spike structures inside the hollow tube to allow more space for faster and unhindered nerve regeneration.

Regenerative electrodes are the most invasive of all electrode types due to the need to sever the nerve prior to electrode placement. However, at the same time, its high invasiveness also brings it an extremely high spatial resolution. For sieve electrodes, the spatial resolution depends on the number of pores in the electrode (Rijnbeek et al., 2018; Yildiz et al., 2020). However, the excessive number of pores will lead to partial demyelination of the myelin at the sieving interface due to axonal contraction, making the reinnervation of the distal motor fibers from the myelinated fibers poor. As a result, distal preservation of muscle mass and muscle force output was significantly impaired (MacEwan et al., 2016).

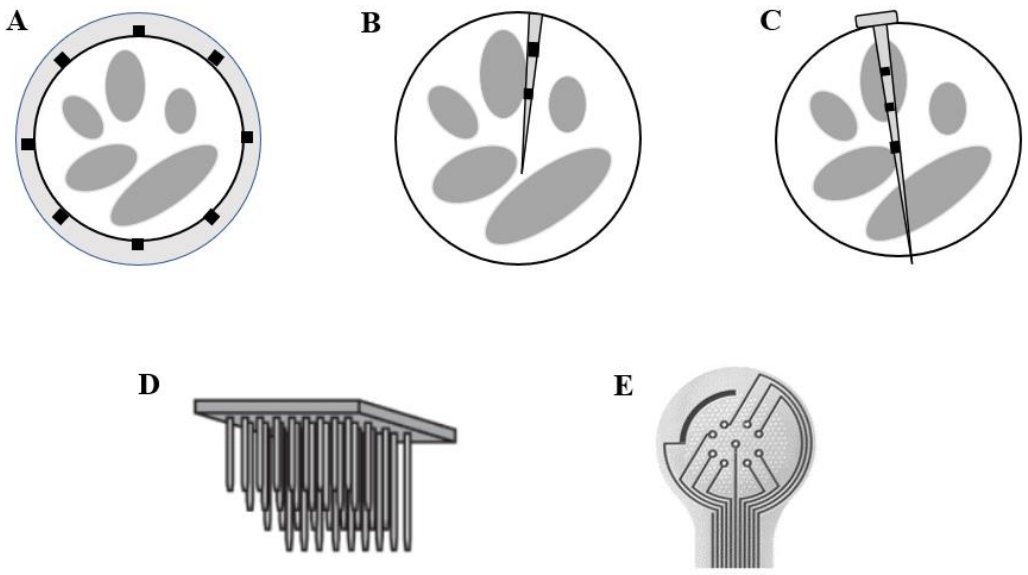

Figure 2.7: (**A**) Cuff Electrode. (**B**) Longitudinal inter-fascicular electrode (LIFE). (**C**) Transverse intra-fascicular multichannel electrode (TIME). (**D**) Utah slanted electrode array (USEA) (adapted from Navarro et al., 2005). (**E**) Regenerative Sieve electrode (adapted from Negredo et al., 2004).

2.5.5 Macro-Sieve Electrodes

As described in the previous section, sieve electrodes provide an interface for stimulating peripheral nerve axons with extremely high spatial resolution. However, to successfully utilize this feature requires excellent regeneration. MacEwan et al. published a paper in 2016 investigating the role of the large transport zone in enhancing axon regeneration. This paper presents a new sieve electrode design, the micro-sieve electrode (MSE), and tests it on the sciatic nerve of male Lewis rats.

The MSE consists of three concentric rings: an inner porous zone and an outer PCB ring (Figure). The inner porous zone is 2 mm in diameter and contains nine transition zones to maximize functional recovery of the nerve. The central transport zone of the porous zone is a circular region with a diameter of approximately 600 μm surrounded by eight diamond-shaped regions. Among them, the central and peripheral transport area's cross-sectional area equals about 0.285 mm^2. MSE has Eight Platinum-iridium conductors, four of which are connected to the central transmission zone of the porous site and are sequentially labeled C1, C2, C3, and C4. The remaining four conductors are in alternating radial spokes and are labeled P1, P2, P3, and P4 (Chandra et al., 2021; MacEwan et al., 2016).

The study by MacEwan et al. demonstrated that the design of MSE can effectively exclude any physical obstacles to axon regeneration while ensuring high spatial resolution of peripheral nerves. The structure of the polyimide wafer and the ultrasonic bonding of the micro-PCB maximize the mechanical stability of the electrodes and ensure the reliability of the internal electrical connections (MacEwan et al., 2016). Chandra et al. 2021 further investigated whether MSE could elicit sensory perception at low current levels in the face of altered morphology and caliber distribution inherent to axon regeneration. This experiment demonstrates that the average

current required for stimulus detection in male Lewis rats is 19.37 μA per channel when using a multi-channel stimulation configuration. On the other hand, the single-channel thresholds of leads near the nerve center averaged half that of those near the periphery (Chandra et al., 2021). This experiment only tested the current required for stimulus detection in male Lewis rats during multi-channel stimulation at a PF configuration of 50 Hz, while the effects of other configurations are unclear. Therefore, similar in vivo assessments of other PF and channel configurations of MSE are required.

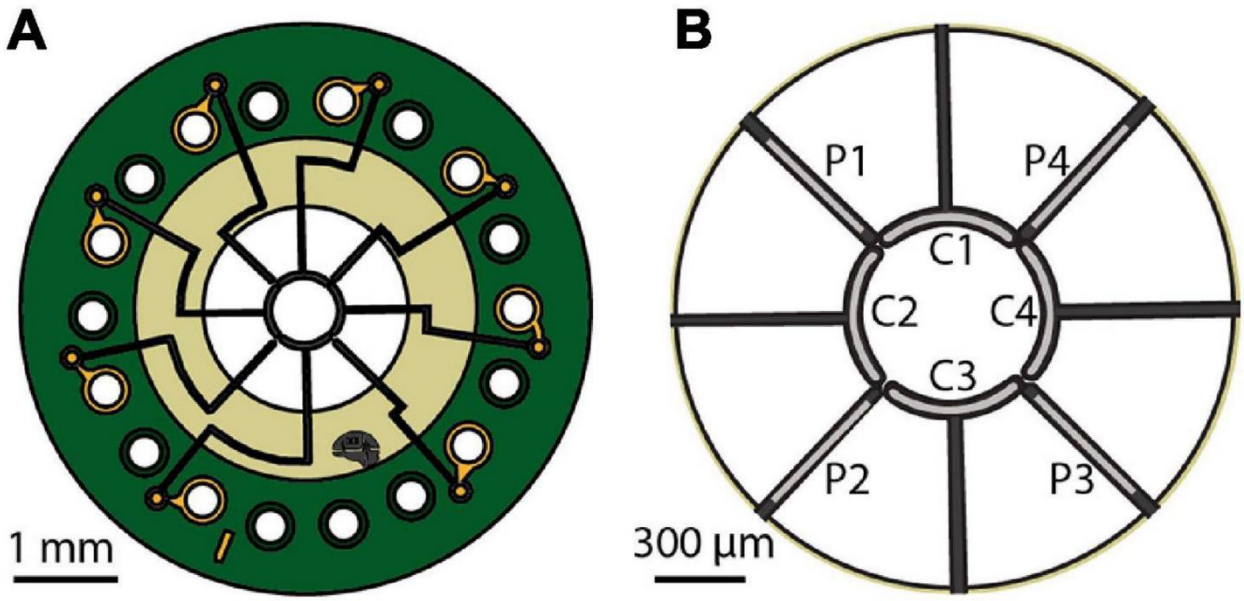

Figure 2.8: (**A**) The macro-sieve electrode. (**B**) Labeled macro-sieve electrode Platinum-iridium conductors (adapted from Chandra et al., 2021).

Chapter 3: Method

The devices and methods used in the experiment followed the original method (Chandra et al., 2021), and only some methods were modified based on different needs. The experimental setup consists of an animal behavior module, an electrophysiology module, and a commutator assembly that delivers stimuli to the implanted MSE. A voltage converter that transmits TTL signals establishes the connection between the electrophysiological module and the electrophysiological module.

3.1 Experimental Apparatus

The detection threshold and slope of different MSE stimulation PF applied to the sciatic nerve were measured by forcing male Lewis rats to learn a discrimination detection task by restricting food. Depending on the settings of the discrimination detection task, the probability of stimulus detection threshold was at 75%. The rats were trained on auditory stimuli before implanting MSE. After the rats successfully detected standard performance (Correct rate>85%) in three consecutive days of training, MSE implantation was performed on the right nerve of the rats. At the time of surgery, rats also underwent a subcutaneous tunnel and head-cup construction. The interior of the head cup contains an embedded connector fixed by dental cement for connection to an external electrophysiological stimulator. The rats underwent auditory stimuli recovery training 4-6 weeks after the operation. After the rats regained standard performance, training began with combined auditory and sciatic stimuli presented synchronously. During the training process, the range of the maximum stimulus acceptable to the rat was judged by the number of tasks performed each time and the behavior in the Skinner box. After a complete pause in auditory stimulation after 4-6 sessions, rats were subsequently trained with a fixed intensity of electrical stimulation until they reached standard performance. The rats will then be sequentially

given random current amplitudes at a given PF. The method will be applied to 5 PF, the initial PF is 50Hz, and each subsequent frequency is twice the previous frequency. The resulting dataset will derive psychometric curves for stimulus detection probability versus current intensity and the calculation of detection thresholds.

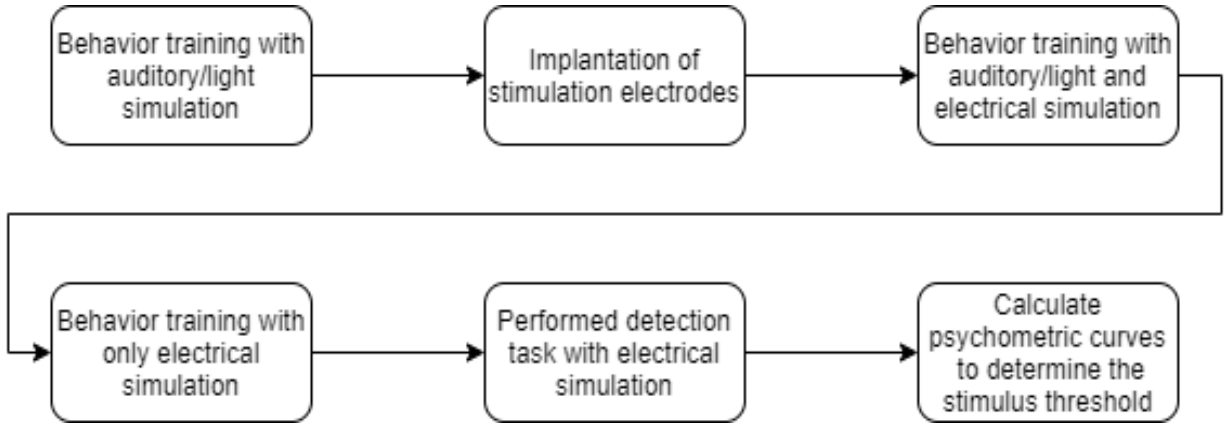

Figure 3.1 Main pipeline of the experimental.

3.1.1 Behavioral Module Hardware

Behavioral modules were constructed using Med Associates, Inc. (St. Albans, VT, United States) and Coulbourn Instruments (Lehigh Valley, PA, United States). The module's body is a modular Skinner box (30.48 cm high, 25.4 cm deep, and 30.48 cm wide). In order to exclude external interference as much as possible, the Skinner box is enclosed in an auditory and light attenuation chamber. The modular panel in the middle of the right wall of the Skinner box (from top to bottom) houses an in-box light, a 2,900 Hz Sonalert (Tone Generator), a 4500 Hz Sonalert (Tone Generator) and a nose detector (2.54cm diameter; 6.35cm from the floor). The modular panels on the left and right of the right box wall are fitted with a rectangular food receptacle (5.75cm wide, 4.45 high, flush with the floor). A 20 mg food pellet dispenser (BioServ, Prospect, CT, USA; #F0163) was attached to each food receptacle. The Skinner box is also equipped with two

external handheld buttons to interfere with dispensing the food pellets of the two food receptacles or the lighting in the box if necessary. Two holes were drilled into the ceiling of the Skinner box to accommodate a webcam and commutator components.

Multiple Skinner boxes are controlled by a Dell Optiplex 790 computer fitted with a DIG-704 PCI card. An SG-716B SmartCtrl connection panel mediates each Skinner box's signal output and input with 16 output and 8 input 3-pin Molex channels. After the signal is conditioned, it will be input to the host computer via the dedicated DIG-716B SmartCtrl interface module and run on the Pascal-based code.

The behavioral module used in the electrical stimulation detection task used two pairs of DIG-716B/SG-716B. The first pair controls the Skinner box, and the second pair relays the signal to a voltage converter designed by Chandra et al. in 2021 to communicate information between the behavioral and electrophysiological modules. **Table 3.1** lists all materials used.

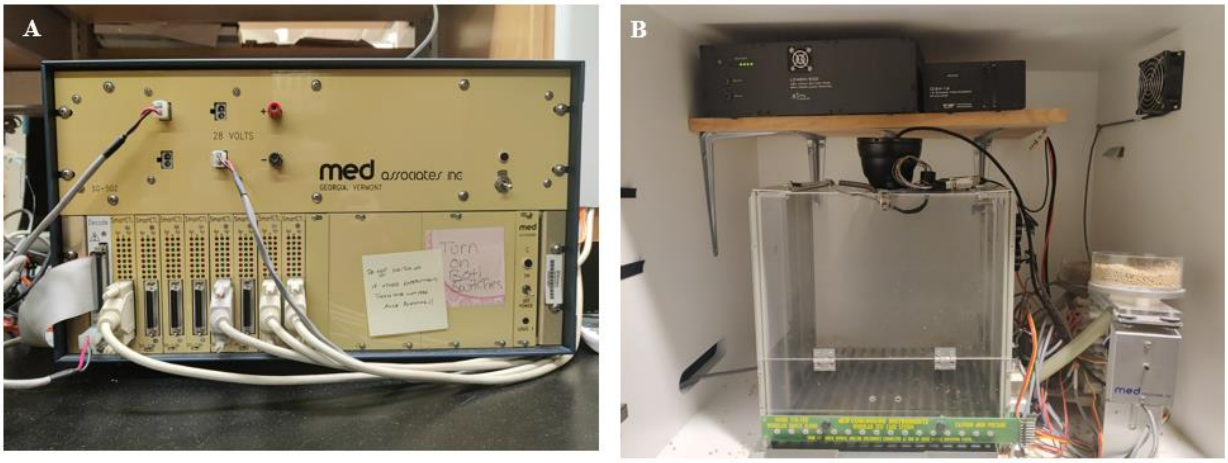

Figure 3.2: (**A**) MED associate SmartCtrl Interface Module. (**B**) Skinner Box.

Table 3.1: Materials used in behavioral module hardware (adapted from Chandra et al., 2021).

Item	**Manufacturer**	**Part Number**
Computer	Dell	Optiplex 790
PCI Card	Med Associates	DIG-704
SmartCtrl Interface Module	Med Associates	DIG-716B
SmartCtrl Connection Panel	Med Associates	SG-716B
Sound and Light Attenuating Chamber	Med Associates	ENV-017M
Modular Test Cage System	Coulbourn Instruments	H10-11R-TC
Shock Floor for Rat Test Cage	Coulbourn Instruments	H10-11R-TC-SF
Drop Pan for Rat Test Cage	Coulbourn Instruments	H10-11R-TC-DP
Nose-Poke Detector	Coulbourn Instruments	H10-09R
Nose-Poke RJ11-to-Molex-Adapter	Coulbourn Instruments	H91-21
Food Magazine	Med Associates, Inc.	ENV-200R2M
Food Magazine Head Entry Detector	Med Associates, Inc.	ENV-254CB
Pellet Dispenser (20 mg)	Med Associates, Inc.	ENV-203-20
House Light	Coulbourn Instruments	E11-01
Tone Generator (2,900 Hz)	Med Associates, Inc.	ENV-223HAM2
Tone Generator (4,500 Hz)	Med Associates, Inc.	ENV-223AM
Hand-Held Push Button	Med Associates, Inc.	SG-205
Webcam	Ailipu Technology Company	ELP-USB100-W05MT-DL36
Fisheye Lens Attachment for Smartphone	Habor	N/A

3.1.2 Electrophysiological Module Hardware

The electrophysiological module consists of three parts, the primary control computer, the RZ5D base station, and the IZ2H-16 stimulus isolator. A Dell XPS 8900 computer was used to control the programming of the electrophysiology module and main program operation. The computer has been fitted with a P05E PCI card to interface with the RZ5D base station. The RZ5D base station connected with the primary control computer drives the IZ2H-16 stimulus isolator powered by the LZ48-500M battery pack through the optical fiber. The IZ2H-16 connects to a custom commutator assembly via a DB26 to DB25 DBF-MiniDBM adapter and delivers electrical stimulation to the rat's implanted electrodes through a connector mounted on the rat's skull.

The RZ5D has a DB25 digital I/O port that interfaces with the voltage converter hardware and communicates with the behavior module. The voltage converter hardware is designed and improved by Chandra et al. in 2021. The voltage converter is designed to step down the 28 V signal from the secondary SG-716B output channel of the behavior module to a TTL signal or boost the TTL signal from the RZ5D digital I/O port to 28 V and input to the SG-716B. **Table 3.2** lists all materials used.

Figure 3.3: (**A**) LZ48M-500 Battery. (**B**) IZ2H-16 Stimulus Isolator. (**C**)RZ5D Base Station.

Table 3.2: Materials used in electrophysiologica module hardware (adapted from Chandra et al., 2021).

Item	**Manufacturer**	**Part Number**
Computer	Dell	XPS 8900
PCI Card	Tucker-Davis Technologies	P05E
Base Station	Tucker-Davis Technologies	RZ5D
Stimulus Isolator	Tucker-Davis Technologies	IZ2H-16
Battery	Tucker-Davis Technologies	LZ48-500M
DB26-to-DB25 Adapter	Tucker-Davis Technologies	DBF-MiniDBM

3.1.3 Commutator

The commutator consists of five parts, including a 12-channel slip-ring commutator (Moog Inc.,

Elma, NY, United States; AC6023), a female connector (Omnetics Connector Corporation,

Minneapolis, MN, United States; #A76855-001), stainless steel spring wrap (Tollman Spring Company, Bristol, CT, United States), a male D-Subminiature 25 (DB25) connector (NorComp Inc., Charlotte, North Carolina, United States; 225ME-ND) and an extension spring (McMaster - Carr, Elmhurst, IL, United States; #9654K513).

The 12-channel slip-ring commutator allows the rat to move freely while remaining connected to the IZ2H stimulation isolator. The upper end of the slip-ring commutator is soldered with the male DB25 connector, which is used to communicate with the electrophysiological module. The lower end is soldered with the female connector for connecting with the male connector of the rat head. The connecting wire between the female connector and the slip-ring commutator is wrapped by stainless steel spring wrap to avoid damage to the connecting wire due to scratching and biting by rats. The connecting line between the female connector and the slip-ring commutator is reserved enough to allow the rat to move freely to the farthest corner of the cage. A tension spring was attached to the outside of the spring wrapped with heat shrink tubing and hot glue to prevent the rat from getting tangled by the wires when moving in the Skinner box. The tension spring formed a semi-circular structure that allowed the cable to release or tighten excess as the rat moved. **Table 3.4** lists all materials used. The production of this component is adapted from Chandra et al., 2021.

The following are the detailed production steps:

Step 1: Remove wires 1 to 6 from the Omnitics connector.

Step 2: Cut the wire 7 to 18 from the Omnitics connector into 36 cm**.**

Step 3: Strip the rubber from the tip of each Omnetics wire to expose 0.8 cm of exposed wire.

Step 4: Thread the Omnetics wire through the 32 cm spring warp.

Step 5: Slip a 1.5 cm long heat shrink tube close to the Omnetics connector and shrink it with a heat gun.

Step 6: Place two 2 cm long heat shrink tubes on the spring warp, then shrink them in **step 11**.

Step 7: The slip ring is divided into an upper end and a lower end, the upper end is wider, and the lower end is narrower. The upper-end lines are divided into two groups, 6 on each side. Solder wires 1, 2, 3, and 4 of the 12 wires to channels 1, 2, 3, and 4 of the male DB25 connector. Solder wires 5 and 6 to channels 7 and 8 of the male DB25 connector. Solder wires 7 and 8 to channels 20 and 21 of the male DB25 connector. Solder wires 9 and 10 to channel 15 of the male DB25 connector. Solder wires 11 and 12 to channel 6 of the male DB25 connector. Use 1.5cm long heat shrink tubing to reinforce and insulate each solder joint. **Table 3.3** identifies the color of each cable and the corresponding DB25 connector channel.

Step 8: Cut the 12 wires at the end of the slip ring to 2.5 cm, then strip the rubber on the tip of each wire to expose 0.8 cm of bare wire.

Step 9: Solder the wires to the Omnitics connector using the numbers and colors provided in **Table 3.3**. Use 1.5 cm long heat shrink tubing to reinforce and insulate each solder joint.

Step 10: Pack all end wires soldered and protected into a large 3.5 cm long heat shrink tube and shrink using a heat gun.

Step 11: Thread the two ends of the extension spring apart through the two unshrank heat shrink tubes from **Step 6**. The distance between the two tubes should be 14 cm. After determining the distance, shrink it with a heat gun.

Step 12: Reinforce the heat shrink tubing used to secure the extension springs near the Omnetics connector with epoxy.

Step 13: Check other heat shrink tubing for looseness and reinforce with a small amount of epoxy, if any.

Table 3.3: Channel mappings for commutator Omnetics connector (adapted from Chandra et al., 2021).

Slip ring wire number	Slip ring wire color	DB25 connector channel	Omnetics Connector wire number	Omnetics Connector wire color
1	BLK	1	11	BLK
2	BRN	2	12	BRN
3	RED	3	13	RED
4	ORN	4	14	ORN
5	YEL	7	15	YEL
6	GRN	8	17	BLU
7	BLU	20	16	GRN
8	VIO	21	18	VIO
9	GRY	15	7	BLU
10	WHT	15	8	VIO
11	WHT-BLK	16	9	GRY
12	WHT-BRN	16	10	WHT

Table 3.4: Materials used in commutator (adapted from Chandra et al., 2021).

Item	Manufacturer	Part Number
Slip Ring Capsules (Compact)	Moog Inc.	AC6023

Latched, Female Connector	Omnetics Connector Corporation	A76855-001
Extension Spring	Extension Spring McMaster-Carr 9654K513	Extension Spring McMaster-Carr 9654K513
Silicone Adhesive	Factor II Inc.	A-564
2-Part Epoxy	Permatex	84101
DB25 D-Sub Connector	NorComp Inc.	225ME-ND
Solder	Multicore	) MM00978
Flux Chip	Quick Inc.	SMD291
Soldering Station	Weller	WX1
Soldering Tip	Weller	5MS, RT 13MS, RT 15 MS

3.1.4 Programming the Behavioral Module

The hardware of the behavior module runs through a programming language called Med-State Notation (MSN). MSN programs are composed of code blocks organized into "state sets." There can be 32 state sets in a program, and each can run concurrently in the same program. The basic building block of a state set is called a "state." In a state set, the program can only run one state at a time. Each state contains one or more sequences of commands to execute when the corresponding condition is met. Each command sequence ends with an instruction to move to another state set in the same state set or to repeat the current state set.

The part of the code that communicates with the Electrophysiological module is based on the system built by Chandra et al. in 2021. In an experiment, the primary and secondary DIG-716B/SG-716B of the Behavior Module and Electrophysiological Module run separate MSN programs in parallel. The main MSN procedure delivers K pulses at stimulus onset, early withdrawal nose-poke detector, correct withdrawal, session start, and session termination. After

issuing one, the secondary MSN program will receive K pulses and trigger the command sequence for the corresponding output channel. Activation of the command sequence triggers the voltage converter to convert the emitted signal to a TTL signal and transmit it to the digital I/O port of the Electrophysiological module RZ5D. Next, the Electrophysiological module will determine whether to deliver electrical stimulation based on the information received. After the action is complete, the Electrophysiological module emits a confirmation signal and returns to the Behavior module through the input channel of the auxiliary DIG-716B/SG-716B.

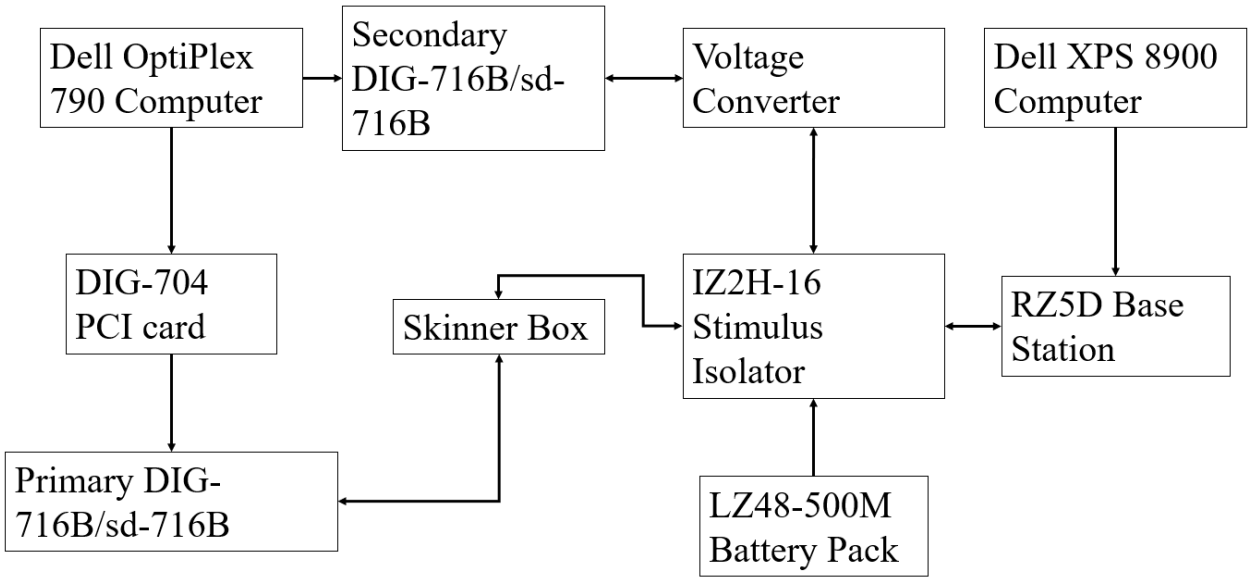

Figure 3.4: Signal exchange pipeline of the experimental equipment (adapted from Chandra et al., 2021).

3.2 The Macro-Sieve Electrode Stimuli Module Assembly

The Macro-Sieve Electrode (MSE) Stimuli Module consists of 5 components, including an MSE, a male connector (Omnetics Connector Corporation, Minneapolis, MN, United States; #A76854-001), a pair of silicone guide catheters (ID: 2 mm; A-M Systems, Sequim, WA, United States,

#808500), a small amount of medical grade silicone adhesive (Factor II, Lakeside, AZ, United States, #A-564) and Parafilm (Bemis Company, Inc., Neena, Wisconsin, USA). **Table 3.6** lists all materials used. The production of this component is adapted from Chandra et al., 2021.

The specific production steps are as follows:

Step 1: Remove wires from Omnitics connector channels 1-6.

Step 2: Cut Omnitics connector channels 7 to 10 to 6.5 cm long and strip all insulation.

Step 3: Cut Omnitics connector channels 11 to 18 to 22 cm long and strip the insulation 0.5 cm from the tips.

Step 4: Solder channels 11 to 18 using a lead-free alloy (96.5% Sn, 3% Ag, 0.5% Cu) and no-clean flux (Chip Quick, Inc., Ancaster, ON, Canada; #SMD291) to the corresponding MSE channel. **Table 3.5** shows the correspondence between them.

Step 5: Use a blade and ruler to cut a pair of 4mm long silicone catheters under the microscope and clean them with isopropanol.

Step 6: Use A-564 silicone adhesive to secure a 4mm long silicone catheter to either side of the MSE polyimide section using A-564 silicone adhesive and cure for 24 hours. Be careful not to allow the adhesive to smear the active area of the MSE. Any intrusion of the adhesive over the polyimide portion may cause some or all channels to fail to pass any current.

Step 7: Repeat Step 6 to secure the remaining 4mm long silicone tubing to the other side of the MSE polyimide section and cure for 24 hours.

Step 8: Apply more silicone adhesive to both sides of the PCB section of the MSE to insulate the solder joints and cure for 24 hours. Repeat this step as many times as necessary

Step 9: Measure the channel impedance at 1 kHz and 5 kHz using the Autolab PGSTAT128N potentiostat. The test will only pass if all channel impedances of the electrode are less than 100 kΩ at 5 kHz.

Step 10: Seal the Omnitics Connector in Parafilm.

Table 3.5: Channel mappings for macro-sieve electrode and DB25 connector (adapted from Chandra et al., 2021).

Omnetics Channel	**Status**	**MSE Channel**	**DB25 Channel**
1 to 6	Remove		
7 and 8	Unsoldered		15
9 and 10	Unsoldered		16
11	Soldered	P3	1
12	Soldered	C4	2
13	Soldered	P4	3
14	Soldered	C1	4
15	Soldered	P1	7
16	Soldered	C2	20
17	Soldered	P2	8
18	Soldered	C3	21

Table 3.6: Materials used in macro-sieve electrode stimuli module (adapted from Chandra et al., 2021).

Item	**Manufacturer**	**Part Number**

Latched, Male Connector	Omnetics Connector Corporation	A76854-001
Macro-Sieve Electrode	NeuroNexus Technologies	N/A
Silicone Conduit	A-M Systems	808500
Silicone Adhesive	Factor II, Inc.	A-564
Parafilm	Bemis Company	N/A
Solder (Sn/AG/CU 96.5/3.0/0.5)	Henkel	C511 97SC 3C 0.38MM G
Flux	Quick, Inc.	SMD291
Soldering Station	Weller	WX1
Soldering Tip	Weller	RT 5MS, RT 13MS, RT 15MS

3.3 Training Rats with Auditory Stimuli

3.3.1 Adaptive training

Five-week-old male Lewis rats (Charles River Laboratories, Wilmington, MA, United States; Strain #004) were used in this study. Male Lewis rats underwent 1-2 weeks of manual handling and Skinner box adaptation after acceptance into a rodent-rearing facility. After acclimatization, the rats were placed on food restriction for complex behavioral training. During the food restriction period, the rats were given a premeasured amount of food that they would typically eat unrestricted for 1 hour each day, with 5g-15g of the food depending on the size of the rat. The body weight of each rat will be checked daily during the period of food restriction. Rats need to be allowed to drop to approximately 80% of their free-feeding value during this protocol and maintained. Rats had unrestricted access to food if body weight dropped below 80%.

3.3.2 Hand-Shaping Stage

The hand-shaping stage is divided into two parts. In the first part, rats will be told to eat from food magazines. During this part of the training, its behavior must be monitored through the webcam at all times. After the start of training, a hand-held button will be used to release food pellets whenever the rat approaches the food magazine. This process causes the rat to quickly associate the magazine with the food pellet. Since the follow-up experiment uses the discrimination task, two food magazines will be in the box. At this stage, however, without intervening in the animal's possible bias, both food magazines release food particles when the hand button is pressed. During the first part of the training period, the rat would likely continue to insert its head into the same magazine waiting for the next pellet to be released. To prevent this, the following food pellet was released only after the rat chose to leave the food magazine completely. This training will be done 1-2 times daily for 3 days, 60 minutes each time.

In the second part, rats need to learn to interact with the nose-poking detector, and the release of particles under this part will depend on the rat's proximity to the detector. The food magazine releases food particles under two conditions, either manually by a hand-held button when the rat approaches the nose poke detector or when the rat places its nose in the nose poke detector to trigger the release of food particles. During training, the indicator light of the nose poke detector is on when the rat does not activate it. When the rat puts its nose in the nose poke detector, the indicator light of the nose poke detector will go off immediately. Then the two food magazines will release food particles and turn on the reminder light, which will go off after 1 second. Rats generally understand the association between nose-poke-probe interaction and particle release upon first training. Once the rats understood the association, subsequent experiments did not

require human intervention. This training will be done 1-2 times daily for 3 days, 60 minutes each time.

3.3.3 Auditory Detection Task

The auditory detection task is divided into two parts. In the first part, rats must learn the association between auditory stimuli and food magazines to introduce the discrimination task. Two kinds of auditory stimuli are used in training: high-frequency (4500Hz) and low-frequency (2900Hz). In this part of the training, when the rat puts its nose in the nose poke detector and the detector indicator light goes out, the Skinner box will no longer release food particles directly but randomly release stimuli. Stimuli were classified into two types, auditory stimulus and no stimulus. When the auditory stimulus is activated, the auditory stimulus will last for 500 milliseconds. At the same time, the food magazine associated with this auditory stimulus will release the food and turn on the cue light. When no stimulus is activated, the stimulus will last for 500 ms. At the same time, the food magazine associated with this stimulus will release the food and turn on the cue light. In order to avoid the bias of rats in the choice of a particular direction, two different sets of settings were used for training. In setting 1, low-frequency auditory stimuli were associated with the left food magazine, and no stimuli were associated with the right food magazine. In setting 2, no stimuli were associated with the left food magazine, and high-frequency auditory stimuli were associated with the right food magazine. All rats tested will be randomly assigned equally to the two set species. There is no penalty for wrong choices during this part of the training. When the rat's performance reaches the standard performance (Correct rate>85%) and maintains for 3 days, it will enter the second part of the training.

The second part of the training introduces additional conditions based on the first part. In order to ensure that rats will not repeatedly activate the nose poke detector to cause unnecessary bugs

or data confusion, a determination of the activation time of the nose poke detector was added to the experiment. In all trials, rats were asked to maintain the insertion of the nose-poke detector for more than 500 ms. The insertion time is divided into three kinds of correct withdrawal (CW, insertion time is equal to 500 ms), late withdrawal (LW, greater than 500 ms), and early withdrawal (EW, less than 500 ms). Skinner box's next move will only be triggered when CW or LW is present. In the event of EW, the Skinner box will remain active for 4 seconds while the nose poke detector light is off and will not contribute to the detection statistics. The stimulus setting of the second part is the same as that of the first part, but after the stimulation is triggered, the indicator light of the food magazine will no longer give a clear prompt. Rats must select the correct food magazine by the presence or absence of auditory stimuli. Only when the rat selects the correct food magazine, the food magazine will release food particles and maintain the current state for 4s. If the rat chooses the wrong food magazine, the food magazine will not release any food particles, and the Skinner box will enter the punishment time, that is, turn off all light sources in the box and keep it for 4s. When the rat's performance reaches standard performance (Correct rate>85%) for 3 days, it will enter the surgery preparation stage.

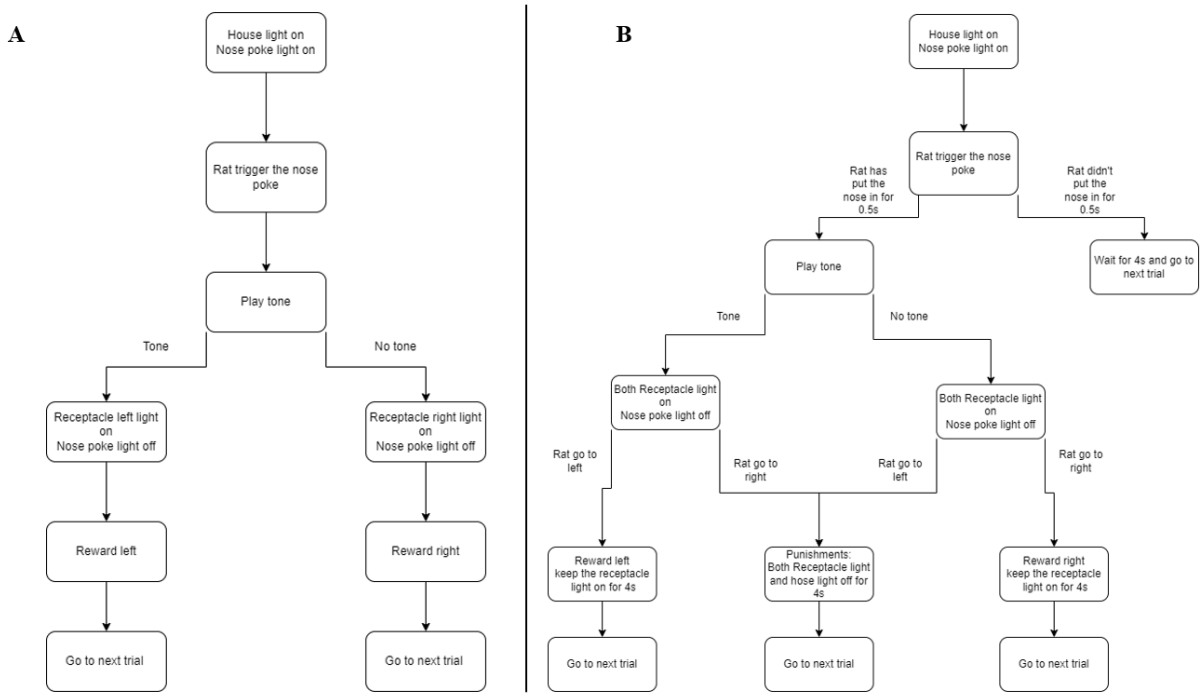

Figure 3.5: (**A**) Pipeline for the first auditory detection task training stage. (**B**) Pipeline for the second auditory detection task training stage.

3.3.4 Bias-correcting Rules

In order to counteract the prevalence of stereotypes, the following bias-correcting rules were used when compiling the auditory detection task and all subsequent tasks (Knutsen, Pietr, Ahissar 2006):

$$|S - O| > |L - R| \rightarrow \begin{cases} S > O \rightarrow O \\ S < O \rightarrow S \end{cases} \quad (3.1)$$

$$|S - O| < |L - R| \rightarrow \begin{cases} L > R \rightarrow R \\ L < R \rightarrow L \end{cases} \quad (3.2)$$

$$|S - O| = |L - R| \rightarrow U([L, R]) \quad (3.3)$$

These rules compare the number of times a rat has approached the same (S) or opposite (O) side in the previous ten trials up to the current trial and the cumulative number of all responses to the

left (L) or right (R) side up to the current trial. An algorithm based on this rule predetermines the type of stimulus that should be given in an upcoming trial when the response ratios to "S"/"O" and "L"/"R" is different. When these ratios were equal, the algorithm randomized the type of stimulus given. Since the same (S) or opposite (O) parameters were calculated in 10 consecutive trials, this makes it difficult to predict upcoming stimulus configurations.

3.4 Implantation of the Macro-Sieve Electrode

MSE implantation was performed on the trained rats when they reached or exceeded the weight of 300 g. The 300 g restriction can improve the survival rate of rats after surgery and reduce the risk of implant failure due to subsequent development. All surgical instruments and implants are sterilized with ethylene oxide or autoclave before surgery.

The surgery was divided into two parts : the head-cap structure construction and the MSE implant implantation. The MSE will be implanted in the rat's right thigh sciatic nerve, and the wire portion of the Omnetics connector will be extended through a subcutaneous tunnel to the rat's head. The Omnetics connector will then be placed into the headgear structure. The construction of the head-cap consisted of a custom-designed cylindrical titanium chamber and a Delrin plastic (DuPont, Wilmington, DE, United States) screw cap. The cylindrical titanium chamber encloses the Omnetics connector and secures it to the rat's head. The Screw caps protect Omnetics connectors from damage or contamination when not in use. **Table 3.7** lists the materials required for the procedure. The production of this component is adapted from Chandra et al., 2021.

The surgical procedure is as follows:

Table 3.7: Materials used in the implantation of the macro-sieve electrode procedure (adapted from Chandra et al., 2021).

Item	Quantity	Manufacture	Part Number
Scalpel	1 unit	-	-
#10 Scalpel Blade	1 unit	-	-
Rat tooth Tweezers	1 pair	-	-
Fine Tweezers	2 pair	-	-
Curved Tunneling Scissors	1 pair	-	-
Suture Driver	1 unit	-	-
Micro-Suture Driver	1 unit	-	-
0-80 1/8” Titanium Skull Screws	4 units	Allied Titanium	Part #0035962
#56 Micro Drill Bits	2 units	McMaster-Carr	
Electric Pin Vise	1 unit	-	-
Ball-End Driver Shaft	1 unit	McMaster-Carr	Part #6972A13
Titanium Chamber	1 unit	-	-
MSE stimuli module	1 unit	-	-
Saline	-	-	-
Cotton-tipped swabs	1-2 bags	-	-
Gauze	1-2 bags	-	-
Pipettes	2 units	-	-
Nylon 8-0 Micro-Suture threads	4-6 units	-	-
4-0 Nylon Suture	-	-	-
5-0 Nylon Suture	-	-	-
Artificial Tears	-	-	-
Retractors	4 units	-	-

Retractor Plate	1 unit	-	-
UV Dental Lamp	1 unit	AZDENT	F*LED-B
Flow-It Dental Acrylic	2-3 tubes	Henry Schein Inc	-
Hydrogen Peroxide	-	-	-
Acetone	-	-	-

Preparation

Step 1: Anesthetize the rat with isoflurane (IH, 4% induction, 2% maintenance).

Step 2: Injection analgesic for postoperative analgesia (buprenorphine SR, administered SC, 1.2 mg/kg).

Step 3: Shave rat's right hind leg, back, and scalp, then repeated disinfection with isopropyl alcohol and Betadine.

Step 4: Apply artificial tears to the eyes of the rats to prevent the eyes from drying out during the procedure.

Step 5: Fix the rat's head in the stereotaxic frame fitted with an appropriate nose cone to deliver isoflurane and oxygen continuously.

Titanium Screws Implantation

Step 6: Use a #10 scalpel to make a sagittal incision along the midline of the rat's head to expose the skull.

Step 7: Scrape bone and soft tissue with the blunt side of the scalpel.

Step 8: Scrub with hydrogen peroxide to remove the blood, and use a small amount of acetone to clean the skull.

Step 9: Drill 4 holes on the skull using a power drill with a #56 micro drill set. Make sure the holes are positioned out of the way of placing the titanium chamber and Omnetics wires.

Step 10: Using a manual pin vise, screw the 0-80 titanium hex screws into the 4 holes. Make sure there is a slight gap between the screw cap and the skull so that the acrylic can penetrate.

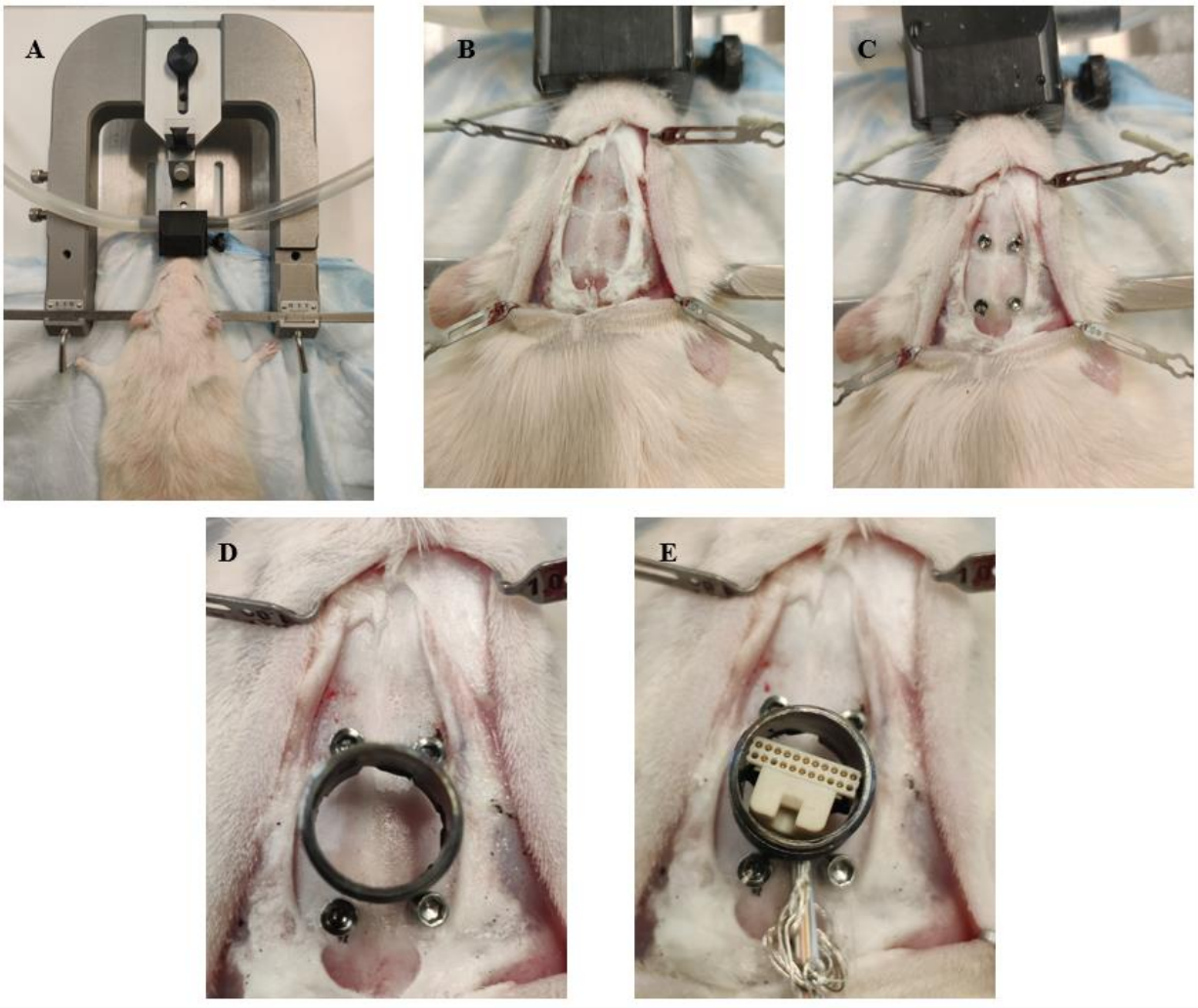

Figure 3.6: (**A**) A rat in the stereotaxic frame. (**B**) Exposure of the skull. (**C**) Four holes are drilled in the skull and a titanium hex screw is screwed into each hole. (**D**) Place the titanium

chamber between the titanium hex screws to ensure proper placement on the skull. (**E**) After the MSE implantation procedure the attached Omnetics connector was passed through the subcutaneous access and placed in the titanium chamber. When filling with acrylic cement, ensure that the locking mechanism is above the upper edge of the titanium chamber.

MSE Implantation

Step 11: Cut the skin and gluteus laterals along a line parallel to the femur.

Step 12: Expose the sciatic nerve by blunt dissection.

Step 13: Transect the sciatic nerve 5 mm proximal to the trigeminal.

Step 14: Nerve stump is placed into the silicone guide catheter of the MSE/Omnetics assembly and sutured using #8 micro sutures

Step 15: Separate the skin and fascia with blunt forceps to create a subcutaneous tunnel from the leg to the scalp incision.

Step 16: Pass the Omnetics Connector through the subcutaneous tunnel to the skull and place it in the protective titanium chamber.

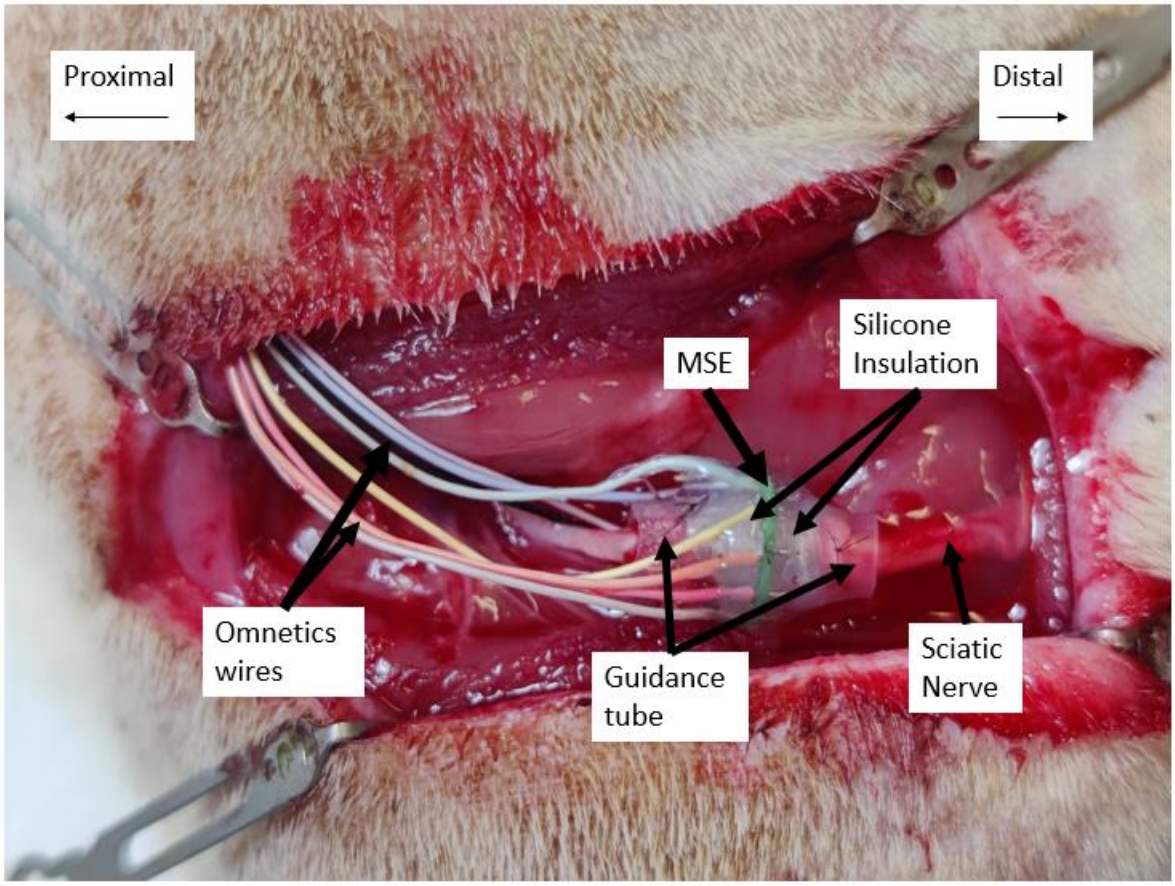

Figure 3.7: Implanted Macro-sieve electrode.

Construction of the head-cap

Step 17: Wrap the entirely stripped Omnetics securely around the titanium screws.

Step 18: Place the titanium chamber containing the Omnetics connectors between the titanium screws and secure the titanium chamber to the titanium screws using Flow-It Dental Acrylic. Cure acrylic with a handheld UV lamp for 30 seconds after application.

Step 19: Carefully introduce the dental acrylic into the interior of the titanium chamber through the 4 notches in the bottom of the titanium chamber, ensuring the Omnetics connector's latching

mechanism is entirely over the edge of the chamber. Make sure not to contaminate the interface portion of the Omnetics connector with any dental acrylic when adding.

Step 20: Make sure that all space between the Omnetics connector and the titanium chamber wall is filled with acrylic, and cure the acrylic with a handheld UV lamp for 30 seconds.

Step 21: Add additional dental acrylic between the titanium chamber and titanium screws to cure the entire structure and cure the acrylic with a hand-held UV lamp for 30 seconds.

Step 22: Seal the titanium chamber with a Delrin screw cap.

Post-Surgical Monitoring

Step 23: After completion of the procedure, use a 5-0 vicryl suture to close the muscle incision, and usa e 4-0 nylon suture to close the skin incision.

Step 24: Rats were returned to their cages, and conditions were monitored every 10 minutes until awakening.

Step 25: Place 1/3 of the cage on a heating pad to create a temperature gradient.

Step 26: Monitor rats daily for 7 days for wound and headgear conformation

Step 27: Remove stitches 8 days after the operation and allow the rat to heal for 4-6 weeks

3.5 Methods for Data Collection

3.5.1 Resumption of Auditory Training

Rats will resume auditory stimulation training 4-6 weeks after surgery. There is no need to shape again during recovery training manually. Rats will be to run the final stage of the auditory detection task again. When the rat's performance reaches the standard (Correct rate>85%) and maintains for 3 days, the rat can start training to transfer to electrical stimulation.

3.5.2 Transferring to Electrical Stimuli

After the recovery training, the rats will perform an auditory detection task containing electrical stimulation. Auditory and electrical stimuli will be presented simultaneously during training, and the electrical stimulation will be a fixed 500 msec, 50 Hz burst of charge-balanced rectangular pulses. Before starting each experiment, in vivo measurements of MSE channel impedance will be performed using TDT's Synapse software suite. In order to find electrical stimulation that elicits a visible twitching response in the legs and feet without overt pain sensation, the intensity of electrical stimulation will be gradually increased (0-100 μA) during training. The training will last for 7 days, and there will be one training session per day, each session will last for one hour.

Next, the rats will be trained to be stimulated only by an electric current of a fixed intensity. The setting of the task is the same as that of the auditory detection task, two different sets of settings were used for training. In setting 1, the electrical stimuli were associated with the left food magazine, and no stimuli were associated with the right food magazine. In setting 2, no stimuli were associated with the left food magazine, and electrical stimuli were associated with the right food magazine. Auditory stimulation was removed entirely from this training to ensure that electrical stimulation would be the only criterion for rats to make decisions. The electrical stimuli intensity will be based on the appropriate intensity found in the previous section to

stimulate the rat. The training will last for 7 days, and there will be one training session per day, each session will last for one hour.

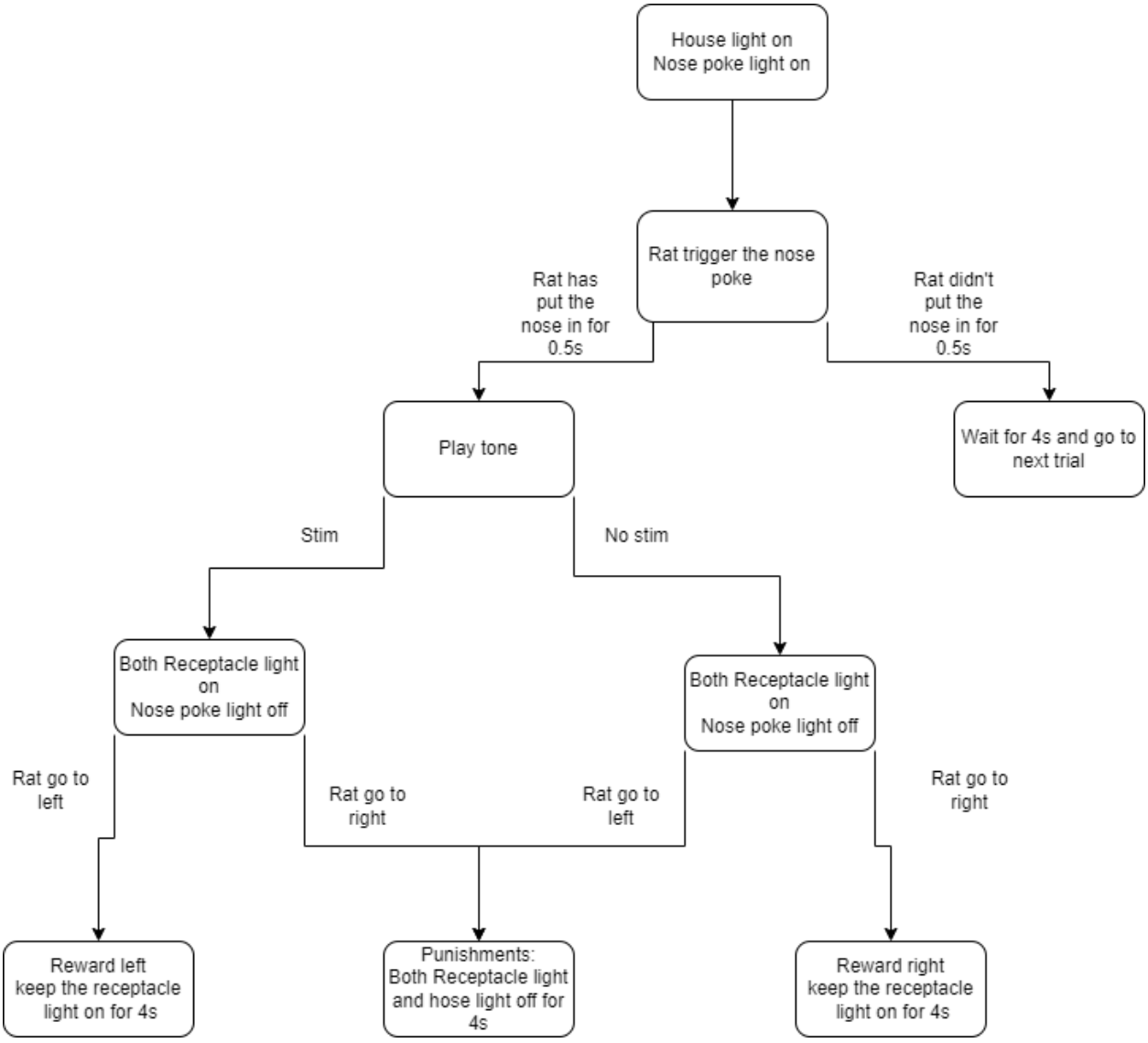

Figure 3.8: Pipeline for electrical stimuli detection task.

3.5.3 The psychometric function

A psychometric function is the most intuitive description of how a psychophysical task affects an observer's behavior. Psychometric functions use $\psi(x)$ as a function expressing the relationship

between performance on a task and stimulus intensity x. In general, academics use F(x; α, β) (or F(x)) to symbolize to describe the probability of identifying the correct stimulus as a function of stimulus x.

The psychometric function is generalized as follows:

$$\psi(x;\theta) = \gamma + (1 - \gamma - \lambda)F(\alpha, \beta) \quad (3.4)$$

Among them, θ refers to the collection of [α, β, γ, λ]. Where α is the threshold and β is the slope or sensitivity. γ is the "guess rate," reflecting the observer's base performance rate in the absence of stimuli. λ is the "lapse rate," which reflects the observer's error response rate regardless of stimulus intensity.

F(x) as a sigmoid function has a variety of optional calculation formulas. The type of stimulation used in this experiment is electrical stimulation, and the final form of electrical stimulation in the living body is electric current. The current function is generally expressed as a logarithmic scale function. Therefore, the Weibull function will be used as the calculation formula of F(x) in the analysis of this experiment. The expression of the Weibull function is as follows:

$$F_w(x;\alpha,\beta) = 1 - \exp\left(-\left(\frac{x}{\alpha}\right)^{\beta}\right) \quad (3.5)$$

with $x \in \{0, +\infty), \alpha \in (0, +\infty), \beta \in (0, +\infty)$.

Where α corresponds to $F_w(x = \alpha;\alpha,\beta) = 1 + \exp(-1) \approx 0.6321$. The parameter β combined with α determines the slope, in which changing the value of α will change the slope of the function even if β remains constant.

Combining the above two formulas, the final expression of the psychometric function in this experiment is:

$$\psi(x;\theta) = \gamma + (1 - \gamma - \lambda)(1 - \exp\left(-\left(\frac{x}{\alpha}\right)^{\beta}\right)) \quad (3.6)$$

Prediction and fitting of the Psychometric Function were done using the *psignifit4* toolbox for Matlab, which implements the Bayesian inference method described by Heiko, et al. (2015).

Chapter 4: Results and Discussion

This experiment was applied to two rats, A and B, over one year. This chapter presents the generation of psychometric curves and the results for thresholds and slopes.

4.1 Collecting the Data

After each rat arrives at the laboratory, it adheres to a predetermined schedule for training and surgery. After completing the rats' adaptive training and hand-shaping stages, the rats will enter the auditory stimulation training stage. The auditory stimulation training phase is divided into two stages. In the first stage, rats will be taught the connection between auditory stimulation and food magazine. The second stage will teach the rats to use the nose poke interval and the time interval between tasks and strengthen the connection between the auditory stimulus and the food magazine.

After the rats had completed auditory training and reached 300 g, surgical implantation of the large sieve assembly and construction of the hood structure of the external connector was performed in the right sciatic nerve in the rat. After the rats had healed for 4-6 weeks, the rats resumed the second stage of auditory stimulation training to strengthen the memory of the training procedure. After completing the recovery training, the rats enter the transition training stage, and the training in this stage will transfer the rats' attention from the auditory stimulation to the electrical stimulation. When the transition training was completed, the rats were given electrical stimulation training to strengthen the task's memory. After completing all training sessions, the rats will perform a detection task of electrical stimuli of different PF.

Table 4.1: Schedule of training, surgery, and data collection for rats A and B.

	Rat A	**Rat B**

	start	end	start	end
Introduce Tones	1/10/2022	1/13/2022	1/11/2022	1/14/2022
Enforce the sound	1/14/2022	3/29/2022	1/17/2022	3/22/2022
Surgery	3/29/2022		3/29/2022	
Enforce the sound	05/06/2022	07/15/2022	05/06/2022	07/11/2022
Enforce the electrical stimulation with sound	07/18/2022	08/31/2022	07/23/2022	09/01/2022
Enforce the electrical stimulation	09/04/2022	09/15/2022	09/06/2022	09/17/2022
Detection Task	09/21/2022	11/14/2022	09/22/2022	11/20/2022

4.2 Analyzing the Data

4.2.1 Rat A

The electrical stimulation detection task of rat A produced five psychometric curves, one for each of 50 Hz, 100 Hz, 200 Hz, 400 Hz, and 800 Hz (see Figure 4.1 and Table 4.2). Since the detection task is yes-no task, the value of guesses correctly is fixed at 0.5 (i.e., 50%). Since rat A refused to accept electrical stimulation above 100 μA during the experiment, data results above this stimulation intensity were excluded. At a PF of 50 Hz, the calculated detection threshold range is 93.760 ± 24.721 μA, and the slope of the threshold is 0.0054 (when the y-axis is a percentage, the conversion slope is 0.54). The observer lapse of the psychometric curve is 0.111 (i.e., 11.1%), so the best correct rate that rat A can achieve is 88.9% at 50 Hz. At a PF of 100Hz, the calculated detection threshold range is 91.635 ± 18.009 μA, and the slope of the threshold is

0.0079 (when the y-axis is a percentage, the conversion slope is 0.79). The observer lapse of the psychometric curve is 0.095 (i.e., 9.5%), so the best accuracy rate that rat A can achieve is 90.5% at 100 Hz. At a PF of 200 Hz, the calculated detection threshold range is 65.304 ± 9.817 μA, and the slope of the g threshold is 0.0093 (when the y-axis is a percentage, the conversion slope is 0.93). The observer lapse of the psychometric curve is 0.039 (i.e., 3.9%), so the best accuracy rate that rat A can achieve is 96.1% at 200Hz. At a PF of 400 Hz, the calculated detection threshold range is 70.170 ± 9.750 μA, and the slope of the threshold is 0.0092 (when the y-axis is a percentage, the conversion slope is 0.92). The observer lapse of the psychometric curve is 0.068 (i.e., 6.8%), so the best correct rate that rat A can achieve is 93.2% at 400 Hz. At a PF of 800 Hz, the calculated detection threshold range is 93.320 ± 22.586 μA, and the slope of the threshold e is 0.0065 (when the y-axis is a percentage, the conversion slope is 0.65). The observer lapse of the psychometric curve is 0.106 (i.e., 10.6%), so the best correct rate that rat A can achieve is 89.4% at 800 Hz.

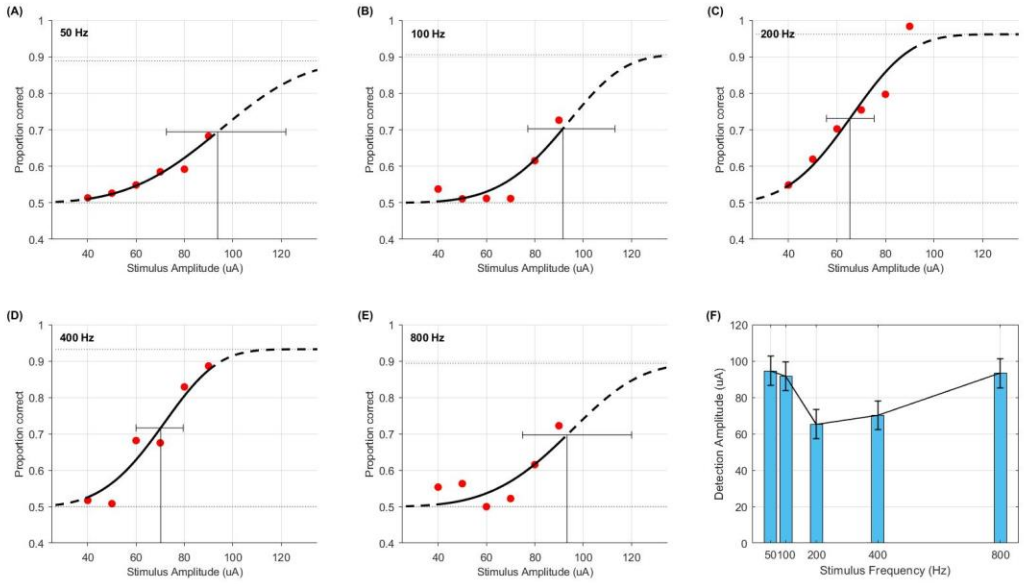

Figure 4.1: (A-E) Psychometric curves of rat A generated by multichannel stimulation at pulse frequencies 50 Hz, 100 Hz, 200 Hz, 400 Hz, and 800 Hz. Error bars represent 95% confidence intervals for the binomial distribution. Threshold, slope, fitting parameters, data dispersion (Extra variance), threshold difference, and ratio are shown in **Table 4.2**. (**F**) The change of rat A's 75% detection threshold with the change of pulse frequency. Error bars represent 95% confidence intervals.

Table 4.2: Threshold, slope, fitting parameters (α β, γ, λ), data dispersion (Extra variance, η), threshold difference, and ratio of rat A generated by multichannel stimulation at pulse frequencies 50 Hz, 100 Hz, 200 Hz, 400 Hz, and 800 Hz shown in **Figure 4.1**.

Frequency (Hz)	**Threshold (α, in μA)**	**Slope (β)**	**Guesses correctly (γ)**	**Observer lapses (λ)**	**Extra variance (η)**	**Threshold Change (μA)**	**Threshold Percent Change**
50	93.760 ± 24.721	0.0054	0.5	0.111	0.0374		
100	91.635 ± 18.009	0.0079	0.5	0.095	0.0421	-2.125	-2.266%
200	65.304 ± 9.817	0.0093	0.5	0.039	0.0749	-26.331	-28.735%
400	70.170 ± 9.750	0.0092	0.5	0.068	0.0540	+4.866	+7.451%
800	93.320 ± 22.586	0.0065	0.5	0.106	0.0461	+23.14	+32.991%

4.2.2 Rat B

The electrical stimulation detection task of rat B produced five psychometric curves, one for each of 50 Hz, 100 Hz, 200 Hz, 400 Hz, and 800 Hz (see Figure 4.2 and Table 4.3). Since the detection task is yes-no task, the value of guesses correctly is fixed at 0.5 (i.e., 50%). Since rat B refused to receive electrical stimulation above 100 μA during the experiment, data results above this stimulation intensity were excluded. At a PF of 50 Hz, the calculated detection threshold range is 95.551 ± 18.567 μA, and the slope of the gate value is 0.0083 (when the y-axis is a

percentage, the conversion slope is 0.83). The observer lapse of the psychometric curve is 0.101 (i.e., 10.1%), so the best accuracy rate that rat B can achieve at 50Hz is 89.9%. At a PF of 100 Hz, the calculated detection threshold range is 989.067 ± 26.867, and the slope of the gate value is 0.0049 (when the y-axis is a percentage, the conversion slope is 0.49). The observer lapse of the psychometric curve is 0.112 (i.e., 11.2%), so the best correct rate that rat B can achieve at 100 Hz is 88.8%. At a PF of 200 Hz, the calculated detection threshold range is 101.452 ± 32.189 μA, and the slope of the gate value is 0.0061 (when the y-axis is a percentage, the conversion slope is 0.61). The observer lapse of the psychometric curve is 0.161 (i.e., 16.1%), so the best correct rate that rat B can achieve at 200Hz is 83.9%. At a PF of 400 Hz, the calculated detection threshold range is 91.385 ± 22.723 μA, and the slope of the gate value is 0.0050 (when the y-axis is a percentage, the conversion slope is 0.5). The observer lapse of the psychometric curve is 0.116 (i.e., 11.6%), so the best correct rate that rat B can achieve at 400 Hz is 88.4%. At a PF of 800 Hz, the calculated detection threshold range is 995.311 ± 41.246 μA, and the slope of the gate value is 0.0046 (when the y-axis is a percentage, the conversion slope is 0.46). The observer lapse of the psychometric curve is 0.182 (i.e., 18.2%), so at 800 Hz, the best correct rate that rat B can achieve is 81.8%.

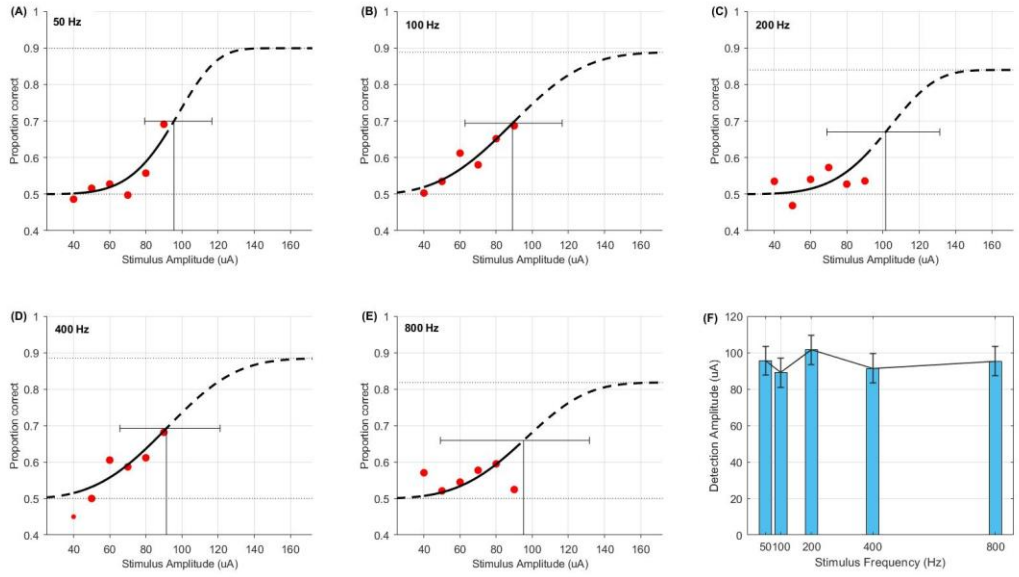

Figure 4.2: (A-E) Psychometric curves of rat B generated by multichannel stimulation at pulse frequencies 50 Hz, 100 Hz, 200 Hz, 400 Hz, and 800 Hz. Error bars represent 95% confidence intervals for the binomial distribution. Threshold, slope, fitting parameters, data dispersion (Extra variance), threshold difference, and ratio are shown in **Table 4.3**. (**F**) The change of rat B's 75% detection threshold with the change of pulse frequency. Error bars represent 95% confidence intervals.

Table 4.3: Threshold, slope, fitting parameters ($\alpha, \beta, \gamma, \lambda$), data dispersion (Extra variance, η), threshold difference, and ratio of rat A generated by multichannel stimulation at pulse frequencies 50 Hz, 100 Hz, 200 Hz, 400 Hz, and 800 Hz shown in **Figure 4.2**.

Frequency (Hz)	**Threshold (α, in μA)**	**Slope (β)**	**Guesses correctly (γ)**	**Observer lapses (λ)**	**Extra variance (η)**	**Threshold Change (μA)**	**Threshold Percent Change**
50	95.551 ± 18.567	0.0083	0.5	0.101	0.0406		
100	89.067 ± 26.867	0.0049	0.5	0.112	0.0400	-6.484	-6.786%
200	101.452 ± 32.189	0.0061	0.5	0.161	0.0428	+12.385	+13.905%

400	91.385 ± 22.723	0.0050	0.5	0.116	0.0451	-10.067	-9.923%
800	95.311 ± 41.246	0.0046	0.5	0.182	0.0497	+3.926	+4.296%

4.3 Discussion

4.3.1 Detection Thresholds Change

As shown in **Figure 4.1** and **Table 4.2**, the detection thresholds of rat A are constantly changing with the stimulation PF. The change of its detection thresholds can be divided into two stages. The first stage was from 50 Hz to 200 Hz, during which the detection thresholds of rat A began to decrease as the PF increased. When the PF increased from 50 Hz to 100 Hz, the detection thresholds of rat A decreased by 2.125 μA, which decreased by 2.266%. When the PF continued to increase from 100 Hz to 200 Hz, the detection thresholds of rat A decreased by 26.331 μA, which decreased by 28.735%. The second stage was from 200 Hz to 800 Hz, during which the detection thresholds of rat A began to increase with signal frequency. When the PF increased from 200 Hz to 400 Hz, the detection thresholds of rat A increased by 4.866 μA, which increased by 7.451%. When the PF increased from 400 Hz to 800 Hz, the detection thresholds of rat A rose back to the approximate level of 50 Hz. During the 400 Hz to 800 Hz period, the detection thresholds increased by 23.14 μA, which increased by 32.991%. From the above data changes, it can be seen that the detection thresholds of rat A have a plateau when the frequency of the stimulation signal changes. When the stimulation PF does not reach the plateau, the detection thresholds of rat A will continue to decline. Once the stimulus PF crosses the plateau, the detection thresholds of rat A will start to rise. According to the available data, this plateau may exist between 200Hz and 400Hz.

As shown in **Figure 4.2** and **Table 4.3**, the detection thresholds of rat B are also changing with the stimulation frequency. However, its detection thresholds lack apparent regularity. In the beginning, the detection thresholds of rat B showed a changing pattern similar to that of rat A. When the PF increased from 50 Hz to 100 Hz, the detection thresholds of rat B decreased by 6.484 μA, which decreased by 6.786%. However, when the PF increased from 100 Hz to 200 Hz, the detection thresholds of rat B changed opposite to that of rat A, and its detection thresholds increased by 12.385 μA, which increased by 13.905%. When the PF increased from 200 Hz to 400 Hz, the detection thresholds of rat B decreased again by 10.067 μA, which increased by 9.923%. Finally, when the PF increased from 400 Hz to 800 Hz, the detection thresholds of rat B rose back to the approximate level of 50 Hz. During the period from 400 Hz to 800 Hz, the detection thresholds increased by 3.926 μA, which increased by 4.296%. From the above data changes, the detection threshold change of rat B is not obvious compared with rat A, but the data trends are similar. From the data trend, the detection thresholds of rat B may have a plateau similar to that of rat A, and this plateau may exist between 100Hz and 400Hz.

4.3.2 Psychometric Function and Data Set

Figures 4.1 and 4.2 show that most of the calculated detection thresholds have very long error bars, and the most significant error can reach ± 41.246 μA. The main reason for this situation is related to the small number of samples and insufficient data width. As mentioned in the method section, prediction and fitting of the Psychometric Function were made using the psignifit4 toolbox for Matlab, described by Heiko et al. (2015). The solid line in Figures 4.1 and 4.2 is the psychometric curve calculated based on actual data points, and the dotted line is the psychometric curve predicted by Bayesian analysis. Some of the calculated detection thresholds are predicted by Bayesian analysis. When predicting, this experiment chooses to rely on the

posterior mean to predict the data. Although it is more reasonable to use the posterior mean from the perspective of Bayesian analysis, due to the small number of samples and insufficient width of some data sets, Bayesian analysis cannot achieve the best prediction. The reasons for the small sample size and insufficient breadth are related to experimental animals and equipment. During the experiment, the rats participating in the experiment did not maintain the same mental state all the time. Generally speaking, the rats participating in this experiment are only willing to participate for one to two hours a day. In some cases, they are completely uncooperative. This situation dramatically limits the amount of data collected in a day. At the same time, because the implanted electrodes and the headgear structure are in the living body for a long time, they will gradually corrode or fail with the passage of time and the activities of the rats. In turn, it will affect the electrode impedance detected on the day. If the impedance changes significantly, it will affect the detection threshold of the rats receiving electrical stimulation. During the data collection, some equipment was repaired and replaced due to the rats' behavior and the aging of the equipment. After the equipment is repaired and replaced, the detected electrode impedance also changes significantly. This makes it necessary to re-collect data once the above situation occurs to exclude the impact of impedance changes. In addition, the amount of data that can be collected in one day is limited, so many invalid data are inevitably generated during the experiment.

4.4 Conclusions

In conclusion, the frequency of multi-channel electrical stimulation signals can considerably impact the detection thresholds of rats from the currently obtained data. In addition, the observed results show that the effect of electrical stimulation PF on detection thresholds is not linear but quadratic, representing a possible plateau for this form of stimulation. However, the specific

cause and more accurate law of this phenomenon still need to be clarified, so further research is required. Suppose the influence of electrical stimulation PF on detection thresholds is properly utilized. In that case, it is predictable that we can combine MSE multi-channel and single-channel stimulation configurations to achieve more complex sensory feedback. These results represent an essential theoretical basis for establishing the feasibility of MSE as a complex sensory feedback interface.

Chapter 5: Future Directions

Previous chapters of this thesis reported changes in MSE detection threshold and slope measurements for different electrical stimulation PF configurations. Despite this success, the experiment still has room for significant improvement. This chapter discusses some experimental refinements and outlines ideas for further experiments to establish the reliability of creating complex sensory feedback based on different electrical stimulation PF configurations.

5.1 Improvement Scheme

As mentioned in the Discussion section, the main problem facing the data in this experiment is the insufficient mount of the data. There is much noise naturally in behavioral experiments, which will directly affect the results of data analysis. There are many ways to denoise data, but all depend on the volume of the data set itself. The more different samples, the more significant the data set and the smaller the noise impact on the final analyzed data. Therefore, more rats need to be tested in follow-up experiments to determine the exact relationship between electrical stimulation PF configurations and detection threshold and the existence of a stimulation plateau.

On the other hand, we can see from the data that the rats participating in this experiment all have a higher detection threshold and a lower maximum acceptable stimulus intensity. The lower maximum acceptable stimulation intensity made the rats refuse to participate in the experiment when the electrical stimulation was more significant than or equal to 100 μA. Due to the higher detection threshold, when the stimulus intensity drops below 40 μA, the correct rate of the task done by the rat under the current PF configuration will always be maintained at about 50% (i.e., the stimulus that cannot be felt). The data collected in this interval is limited. In some cases, rats cannot participate in 75% or more of the task under the current PF configuration of 90 μA electrical stimulation. This lack of data significantly impacts the maximum likelihood estimation

of psychometric curves. The above situation is very different from previous experiments. In previous experiments, rats had a lower detection threshold at 50Hz than reported in this paper (Chandra et al., 2021). The reason for this difference may be related to the experimental design. Although the task used in the experiment is designed to reference two alternative forced choices (2AFC), it is still a yes-no task. The yes-no task is usually considered "criterion-dependent", that is, it depends on the observer's capture of the criteria's features. Because of individual differences, observers tend to use different criteria for judging how strong a signal is received before they answer "yes." Different observers' criteria lead to different biases towards yes or no, regardless of the strength of internal signals (Frederick & Nicolaas, 2016). Therefore, in subsequent experiments, we should consider redesigning a new detection task with 2AFC or 4AFC to eliminate the noise caused by "criterion-dependent."

Finally, future experiments should consider improving the training procedure for rats to shorten the time required. As shown in Table 4.1, it took two rats nearly 10 months from the beginning of the auditory detection task to the electrical stimulation detection task. Excluding the impact of equipment maintenance, the preparation training for the electrical stimulation detection task (auditory detection task to electrical stimulation detection task and enforce the electrical stimulation) also lasted 8 months. The auditory detection task training aims to familiarize the rats with the experimental setup and understand the electrical stimulation based on this. However, since rats need to be trained to enforce the electrical stimulation with sound after surgery, the preoperative auditory detection task becomes less critical. Therefore, skipping the auditory detection task training phase can be considered in future experiments. Instead, the operation will be performed directly after the rats complete the hand-shaping stage, and the electrical

stimulation with auditory training will be now enforced after recovery. This way, the experiment can have more time for the final electrical stimulation detection task and train more rats.

5.2 Future Direction

In the long run, there are two main directions for future performance testing and demonstration of MSE. The first direction is to use more rats based on previous experiments to determine the exact law of the influence of electrical stimulation PF configurations on the detection threshold and the specific range of stimulation plateau. The second direction is to test the performance of this rule in MSE single-channel stimulation and to establish a single-channel stimulus discrimination task of 2AFC. This task will assess whether this regularity produces the same detection threshold difference between the core and peripheral channels of the MSE as in previous experiments (Chandra et al., 2021) and whether this selective difference can be translated into the ability to evoke multiple discernible sensations. After completing the tests on the above two points and collecting enough data, the project should consider using these data to build a neural network model to predict the detection threshold in the future. This model is envisioned to gradually improve with the changes in experimental animal models and finally constitutes an algorithm model that can be applied to sensory feedback correction of upper-limb prosthetics.

References

A. KFA, Prins N. *Psychophysics: A Practical Introduction*. BOSTON, MA: Elsevier - Academic Press; 2016.

Antfolk C, D'Alonzo M, Rosén B, Lundborg G, Sebelius F, Cipriani C. Sensory feedback in upper limb prosthetics. *Expert Review of Medical Devices*. 2013;10(1):45-54. doi:10.1586/erd.12.68

Ayub R, Villarreal D, Gregg RD, Gao F. Evaluation of transradial body-powered prostheses using a robotic simulator. *Prosthetics & Orthotics International*. 2017;41(2):194-200. doi:10.1177/0309364616650077

Biddiss EA, Chau TT. Upper limb prosthesis use and abandonment: A survey of the last 25 years. *Prosthetics and Orthotics International*. 2007;31(3):236-257. doi:10.1080/03093640600994581

Chandra NS, McCarron WM, Yan Y, et al. Sensory percepts elicited by chronic macro-sieve electrode stimulation of the rat sciatic nerve. *Frontiers in Neuroscience*. 2021;15. doi:10.3389/fnins.2021.758427

Das N, Nagpal N, Bankura SS. A review on the advancements in the field of upper limb prosthesis. *Journal of Medical Engineering & Technology*. 2018;42(7):532-545. doi:10.1080/03091902.2019.1576793

Geng B, Dong J, Jensen W, Dosen S, Farina D, Kamavuako EN. Psychophysical evaluation of subdermal electrical stimulation in relation to prosthesis sensory feedback. *IEEE Transactions on Neural Systems and Rehabilitation Engineering*. 2018;26(3):709-715. doi:10.1109/tnsre.2018.2803844

Hadzic A. *Regional Anesthesia and Acute Pain Management*. New York, NY: McGraw-Hill Medical; 2007.

Hernigou P. Ambroise Paré IV: The early history of artificial limbs (from robotic to prostheses). *International Orthopaedics*. 2013;37(6):1195-1197. doi:10.1007/s00264-013-1884-7

Li M, Zhang D, Chen Y, et al. Discrimination and recognition of phantom finger sensation through transcutaneous electrical nerve stimulation. *Frontiers in Neuroscience*. 2018;12. doi:10.3389/fnins.2018.00283

MacEwan MR, Zellmer ER, Wheeler JJ, Burton H, Moran DW. Regenerated sciatic nerve axons stimulated through a chronically implanted macro-sieve electrode. *Frontiers in Neuroscience*. 2016;10. doi:10.3389/fnins.2016.00557

Navarro X, Krueger TB, Lago N, Micera S, Stieglitz T, Dario P. A critical review of interfaces with the peripheral nervous system for the control of neuroprostheses and Hybrid Bionic

Systems. *Journal of the Peripheral Nervous System*. 2005;10(3):229-258. doi:10.1111/j.1085-9489.2005.10303.x

Negredo P, Castro J, Lago N, Navarro X, Avendaño C. Differential growth of axons from sensory and motor neurons through a regenerative electrode: A stereological, Retrograde Tracer, and functional study in the rat. *Neuroscience*. 2004;128(3):605-615. doi:10.1016/j.neuroscience.2004.07.017

Rijnbeek EH, Eleveld N, Olthuis W. Update on peripheral nerve electrodes for closed-loop neuroprosthetics. *Frontiers in Neuroscience*. 2018;12. doi:10.3389/fnins.2018.00350

Russell C, Roche AD, Chakrabarty S. Peripheral nerve bionic interface: A review of Electrodes. *International Journal of Intelligent Robotics and Applications*. 2019;3(1):11-18. doi:10.1007/s41315-019-00086-3

Schofield JS, Evans KR, Carey JP, Hebert JS. Applications of sensory feedback in motorized upper extremity prosthesis: A Review. *Expert Review of Medical Devices*. 2014;11(5):499-511. doi:10.1586/17434440.2014.929496

Schultz AE, Kuiken TA. Neural interfaces for control of upper limb prostheses: The State of the art and future possibilities. *PM&R*. 2011;3(1):55-67. doi:10.1016/j.pmrj.2010.06.016

Schütt H, Harmeling S, Macke J, Wichmann F. Psignifit 4: Pain-free bayesian inference for psychometric functions. *Journal of Vision*. 2015;15(12):474. doi:10.1167/15.12.474

Sheehan TP, Gondo GC. Impact of limb loss in the United States. *Physical Medicine and Rehabilitation Clinics of North America*. 2014;25(1):9-28. doi:10.1016/j.pmr.2013.09.007

Stewart JD. Peripheral nerve fascicles: Anatomy and clinical relevance. *Muscle & Nerve*. 2003;28(5):525-541. doi:10.1002/mus.10454

Svensson P, Wijk U, Björkman A, Antfolk C. A review of invasive and non-invasive sensory feedback in upper limb prostheses. *Expert Review of Medical Devices*. 2017;14(6):439-447. doi:10.1080/17434440.2017.1332989

Trent L, Intintoli M, Prigge P, et al. A narrative review: Current upper limb prosthetic options and Design. *Disability and Rehabilitation: Assistive Technology*. 2019;15(6):604-613. doi:10.1080/17483107.2019.1594403

Wichmann FA, Hill NJ. The psychometric function: I. Fitting, sampling, and goodness of fit. *Perception & Psychophysics*. 2001;63(8):1293-1313. doi:10.3758/bf03194544

Yildiz KA, Shin AY, Kaufman KR. Interfaces with the peripheral nervous system for the control of a neuroprosthetic limb: A Review. *Journal of NeuroEngineering and Rehabilitation*. 2020;17(1). doi:10.1186/s12984-020-00667-5

Ziegler-Graham K, MacKenzie EJ, Ephraim PL, Travison TG, Brookmeyer R. Estimating the prevalence of limb loss in the United States: 2005 to 2050. *Archives of Physical Medicine and Rehabilitation*. 2008;89(3):422-429. doi:10.1016/j.apmr.2007.11.005